Tectonics

RESEARCH ARTICLE
10.1029/2019TC005621

Special Section:
The Arctic: An AGU Joint Special Collection

Exhuming the Top End of North America: Episodic Evolution of the Eurekan Belt and Its Potential Relationships to North Atlantic Plate Tectonics and Arctic Climate Change

Agni Vamvaka[1], Jörg Pross[2], Patrick Monien[1], Karsten Piepjohn[3], Solveig Estrada[3], Frank Lisker[1], and Cornelia Spiegel[1]

[1]Department of Geosciences & MARUM, University of Bremen, Bremen, Germany, [2]Institute of Earth Sciences, Ruprecht-Karls-Universität Heidelberg, Heidelberg, Germany, [3]Federal Institute for Geosciences and Natural Resources, Geozentrum Hannover, Hannover, Germany

Abstract We present the first low-temperature thermochronology data from northernmost Ellesmere Island (Canadian Arctic), along with palynological data from Paleogene sediments. Our study area is part of the >2,500-km-long Eurekan deformation belt that formed across the High Arctic during the Eocene. The aim of this study is to investigate the exhumation of the Eurekan belt and potential relationships with the opening of the North Atlantic, as well as with environmental changes of the Arctic. Our data show that the Canadian Arctic margin was characterized by stretching and basin formation during the Paleocene. Sediment deposition occurred in a coastal swamp environment under a warm and humid climate that lasted into the early Eocene. Exhumation of northern Ellesmere Island was episodic and was presumably controlled by strike-slip movements along the De Geer Fracture Zone between Svalbard and Greenland. Enhanced exhumation of northern Ellesmere Island occurred ~66–60 Ma, ~55–48 Ma, 44–38 Ma, and 34–26 Ma. These exhumation periods largely correlate with changes of spreading rates and movement directions of the Norwegian-Greenland Sea. Main topographic growth along the Eurekan belt was temporally coincident with deposition of ice-rafted debris off eastern Greenland. We suggest that Eurekan topography growth was an important trigger for glacier formation in Greenland. The cessation of rapid exhumation at ~26 Ma can be explained by continental separation between Greenland and Svalbard, which decoupled northern Ellesmere Island from strike-slip movements along the De Geer Fracture Zone, eventually leading to the opening of the Fram Strait.

Key Points:
- Thermochronology data suggest Eocene high-latitude rapid exhumation and topography formation
- Intracontinental Eureka Orogeny seems to be controlled by far-field effects of North Atlantic spreading
- Rise of the Eureka Belt starts at warm and humid conditions and may have triggered subsequent Arctic glaciation

Supporting Information:
- Supporting Information S1

Correspondence to:
A. Vamvaka and C. Spiegel,
vamvakaa@uni-bremen.de;
spiegelc@uni-bremen.de

Citation:
Vamvaka, A., Pross, J., Monien, P., Piepjohn, K., Estrada, S., Lisker, F., & Spiegel, C. (2019). Exhuming the top end of North America: Episodic evolution of the Eurekan belt and its potential relationships to North Atlantic plate tectonics and Arctic climate change. *Tectonics*, *38*, 4207–4228. https://doi.org/10.1029/2019TC005621

Received 24 APR 2019
Accepted 29 AUG 2019
Accepted article online 06 SEP 2019
Published online 11 DEC 2019

1. Introduction

The Eocene was a time of profound change in the Arctic, both in terms of tectonics and in terms of climatic evolution. Tectonically, the Arctic was dominated by the Eurekan deformation, which was caused by the northward movement of Greenland, forming a ~2,500-km-long deformation belt along the Canadian Arctic Archipelago, North Greenland, and Svalbard (Tessensohn & Piepjohn, 2000; Thorsteinsson & Tozer, 1970; Figure 1). Also during the Eocene, the Arctic experienced profound climate change. Whereas subtropical conditions prevailed at the beginning of the Eocene (Eberle & Greenwood, 2012; Sluijs et al., 2006), substantially cooler conditions with evidence for seasonal sea ice and at least isolated glaciers are documented for middle and late Eocene, respectively (Eldrett et al., 2007; Stickley et al., 2009; Tripati et al., 2008). Here, we test the hypothesis that the regional tectonic evolution and associated growth of topography provided the nucleus for glacier formation on Arctic land masses, triggering Arctic continental cooling in concert with the global cooling trend during the Eocene (Zachos et al., 2001).

Although the general structural framework of the Eurekan orogeny is reasonably well understood (e.g., Piepjohn et al., 2016), only few data are available on the detailed temporal and spatial evolution of the Eurekan belt and its associated exhumation patterns. Exhumation histories provide indirect estimates for topographic evolution, assuming that the formation of topography is often associated with increasing exhumation rates and that low-lying, tectonically quiet areas are characterized by low exhumation rates. Additional mechanisms that may cause increased exhumation are tectonic denudation and climatic changes.

10.1029/2019TC005621

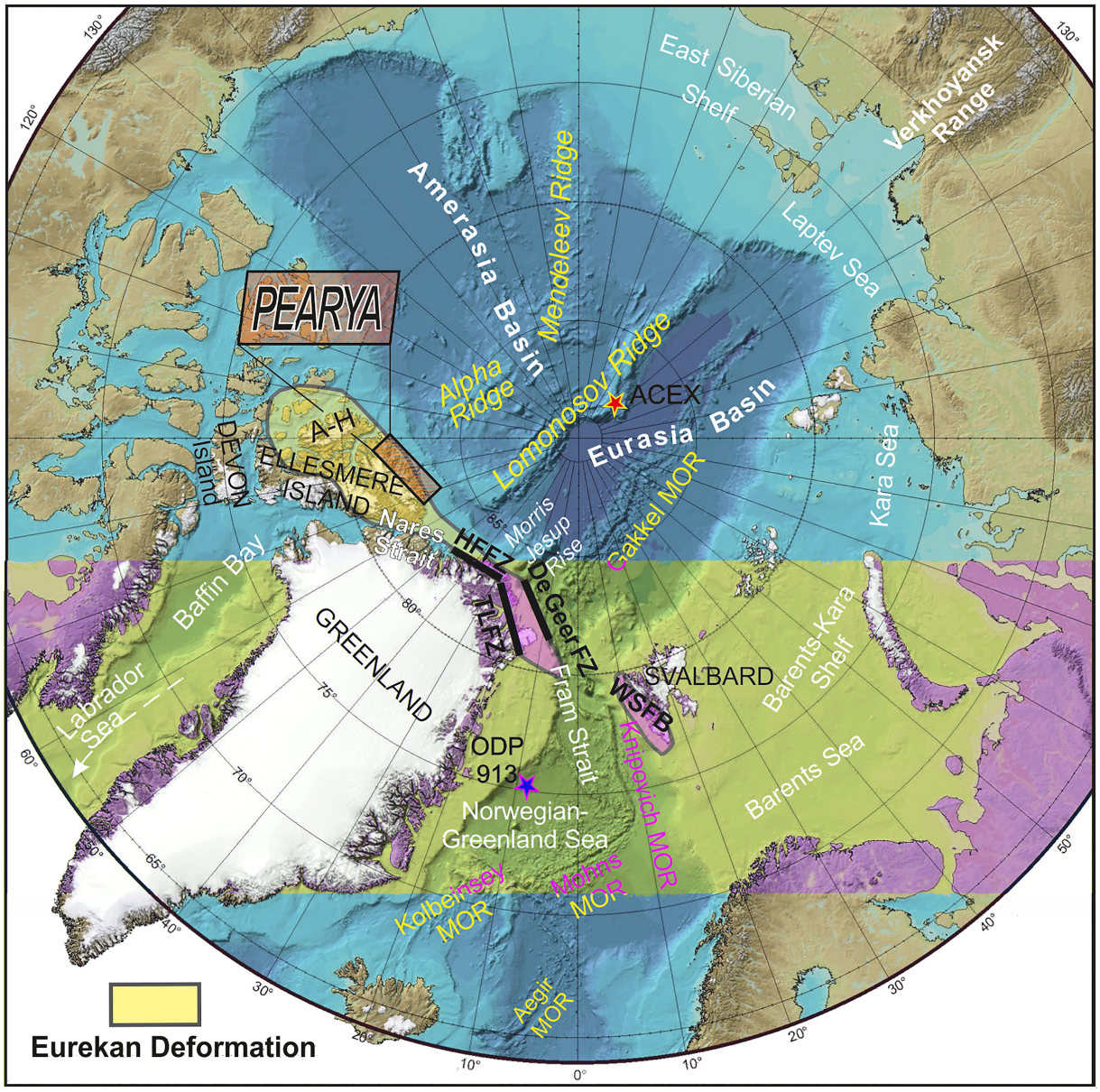

Figure 1. Overview map of the Arctic realm, based on the International Bathymetric Chart of the Arctic region (Jakobsson et al., 2008). The area affected by the Eurekan deformation is highlighted in yellow, and the Pearya terrane is indicated by a black rectangle. Also indicated are ODP site 913 and the IODP site of the Arctic Coring Expedition (ACEX, red stars). The Trolle Land Fault Zone (TLFZ) is interpreted as part of the larger DeGeer Fault Zone (DeGeer FZ). A-H: Axel-Heiberg Island, HFFZ: Harder Fjord Fault Zone, MOR: Mid-Ocean Ridge, WSFB: West Spitsbergen Foldbelt.

Exhumation rates can be derived from low-temperature thermochronology data. Previously published thermochronology data suggest that south and southeast Ellesmere Island experienced little exhumation in response to Eurekan deformation (Figure 2; Grist & Hansen, 2005; Zentilli et al., 2011) and that most Eurekan exhumation seems to have been focused along the large fault systems and toward the north (Arne et al., 1998; Arne et al., 2002).

For this study, we investigated the Pearya terrane, situated adjacent to the Arctic Ocean along the northern rim of Ellesmere Island, forming the northernmost margin of the North American continent (Figure 1). We used apatite fission track (AFT) and (U-Th-Sm)/He (AHe) thermochronology on bedrock and sedimentary exposures to derive the tectonothermal history of that area. We furthermore analyzed sedimentary rocks to derive stratigraphic ages and environmental conditions during deposition. The results are interpreted in the

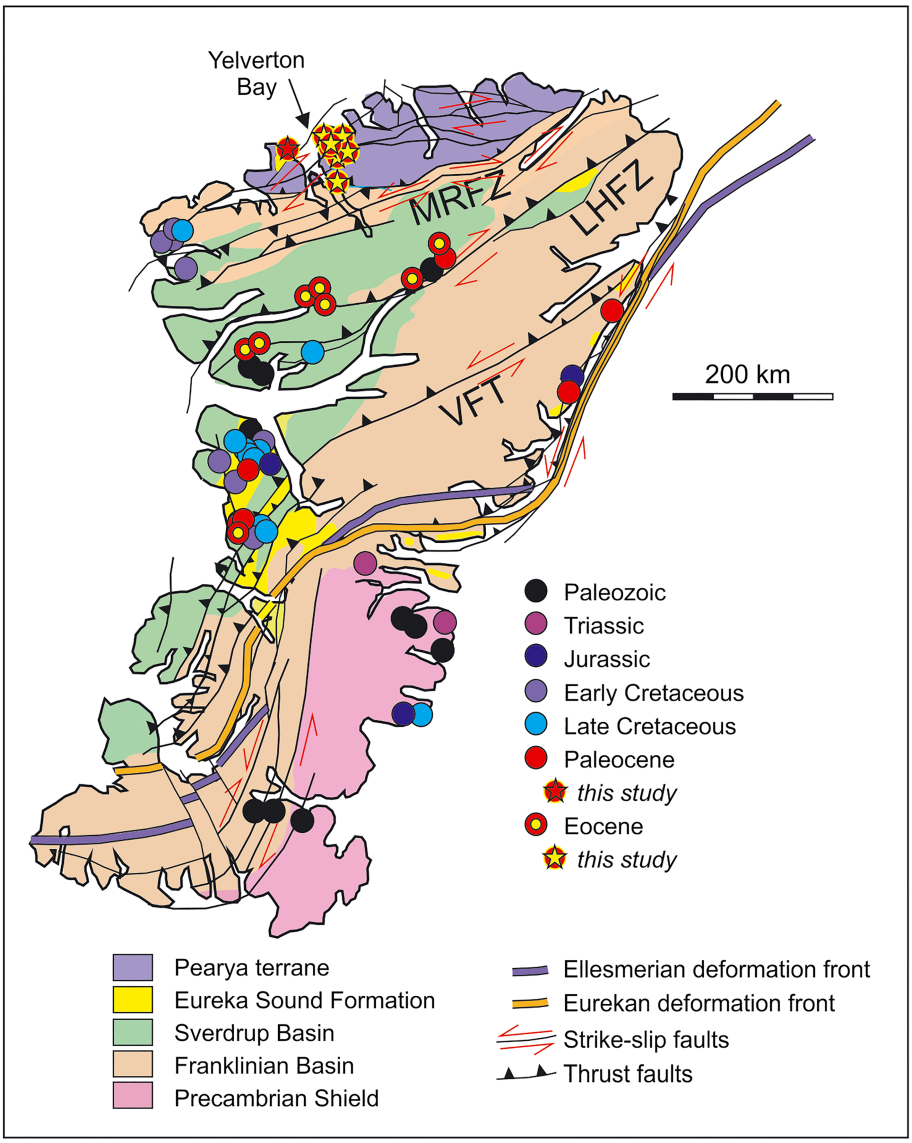

Figure 2. Simplified geological map of Ellesmere Island, showing apatite fission track (AFT) ages of surface outcrops (filled circles) compiled from previously published studies (Arne et al., 1998, 2002, Grist & Zentilli, 2005; Hansen et al., 2011) and from this study (circles with stars) MRFZ: Mount Rawlinson Fault; LHFZ: Lake Hazen Fault Zone; VFT: Vesel Fiord Thrust. Positions of the Ellesmerian and Eurekan deformation fronts are taken from Piepjohn et al. (2015).

context of the existing geophysical, structural, and climatic data. In more detail, we address the following questions: Was northern Ellesmere Island associated with a stronger exhumation response to Eurekan tectonics, as compared to southern Ellesmere Island? If so, when did exhumation take place, how was it related to exhumation of other parts of the Eurekan Belt such as Svalbard, and are exhumation periods of Ellesmere Island temporally correlated with plate tectonic changes of the North Atlantic region and with climatic change in the Arctic realm?

2. Geological Setting

2.1. Structural Framework of the Eurekan

In the following description, we adapt the structural history proposed by Piepjohn et al. (2016, and references therein). In particular, we define the term *Eurekan* as summarizing tectonic activity related to the movement of Greenland as an independent plate, that is, with sea floor spreading active east and west of

Greenland. Therefore, the Eurekan deformation period is defined as of Eocene age, whereas deformation events prior to the independent movement of Greenland (i.e., pre-Eocene) are referred to as *pre-Eurekan* and tectonic activity postdating independent movements of Greenland (i.e., post-Eocene) is defined as *post-Eurekan*).

Ellesmere Island is separated from Greenland by the Nares Strait and the northern Baffin Bay (Figure 1). To the north, it is bordered by the Arctic Ocean, which comprises the older Amerasia Basin formed during the Mesozoic and the younger Eurasia Basin formed from the Eocene onward. Rifting of the Amerasia Basin may have approximately lasted between 195 and 143 Ma and seafloor spreading between 143 and 120 Ma (Alvey et al., 2008; Shephard et al., 2013). The Amerasia and Eurasia basins are separated by the Lomonosov Ridge, a continental sliver formerly situated along the Barents-Kara Shelf (Brozena et al., 2003). During the earliest Cenozoic, Ellesmere Island, Greenland, and Svalbard formed a coherent continental area (Srivastava, 1978).

In the Paleocene, spreading in the Baffin Bay/Labrador Sea commenced (Oakey & Chalmers, 2012; Srivastava, 1978), causing northeastward movement of Greenland relative to North America. This movement was associated with strike-slip faulting and rift-related magmatic activity (i.e. *pre-Eurekan stage*; Piepjohn et al., 2016). The Canadian Arctic must have experienced significant (trans)extension from the Late Cretaceous till at least the end of the Paleocene, as suggested by interpretations of structural data along the Nares Strait (Piepjohn et al., 2016) and of potential field data from the westernmost Ellesmere and Axel Heiberg islands (Anudu et al., 2016). An extensional regime in the Paleocene has also been assumed for a GPlates model (Gion et al., 2017), providing reconstructions with an estimated value of ~85 km of extension between Ellesmere and Devon Islands and of ~20 km of extension between Ellesmere and Axel Heiberg Islands (Harrison, 2006).

In the beginning of Eocene, seafloor spreading in the Norwegian-Greenland Sea initiated (Gaina et al., 2009; Kristoffersen & Talwani, 1977; Srivastava, 1978). Accordingly, two spreading ridges were active east and west of Greenland, so that Greenland moved as an independent plate, marking the beginning of the Eurekan deformation period (Tessensohn & Piepjohn, 2000). The northeastward movement of Greenland resulted in compression between Svalbard and Greenland, initiating the formation of the West Spitsbergen Fold Belt along the western margin of Svalbard (De Geer, 1909; Harland, 1969; Tessensohn & Piepjohn, 2000). The onset of compression between Svalbard and Greenland is assigned to the Early Eocene and defined as *Eurekan Stage 1*, timed as having occurred between ~53 and 47 Ma by Piepjohn et al. (2016). Also at that time, the transtensional regime that has prevailed in the Nares Strait area between Greenland and Ellesmere Island during the Paleocene changed to transpression.

In middle Eocene, the direction of movement of Greenland changed toward the northwest, and, as a consequence, compression along the western margin of Svalbard changed to transpression, and transpression between Ellesmere Island and Greenland changed to compression (cf. *Eurekan Stage 2*; Piepjohn et al., 2016, defined for the time between 47 and 34 Ma). Finally, around the Eocene-Oligocene boundary, seafloor spreading of the Baffin Bay/Labrador Sea ceased and Greenland became part of the North American plate (Kristoffersen & Talwani, 1977), ending Eurekan deformation in a strict sense. With the end of Labrador Sea/Baffin Bay spreading, transpression along West Svalbard changed to transtension, and eventually, the Fram Strait opened, separating Greenland from Eurasia and connecting the Arctic Ocean with the North Atlantic. This last post-Eocene (trans-)tensional stage is referred to as post-Eurekan in the literature (Piepjohn et al., 2016).

2.2. Geology of Ellesmere Island and the Pearya Terrane

In a simplified view, Ellesmere Island comprises five major geological units (defined according to Trettin, 1991; Figure 2): (i) Precambrian rocks of the Canadian-Greenland Shield, exposed in the southeast. (ii) The Franklinian Basin, which contains sediments deposited between the Neoproterozoic and the Devonian at the former passive margin of the Laurentia continent. (iii) The Pearya terrane, along the northern margin of Ellesmere Island, accreted to the Laurentian margin during the Devonian to early Carboniferous Ellesmerian orogeny, which in turn caused the inversion of the Franklinian Basin. (iv) The Sverdrup Basin, formed in the core region of the former Ellesmerian orogen. It contains Carboniferous to Paleogene sediments, deformed during the Eurekan orogeny. (v) The Late Cretaceous to Paleogene

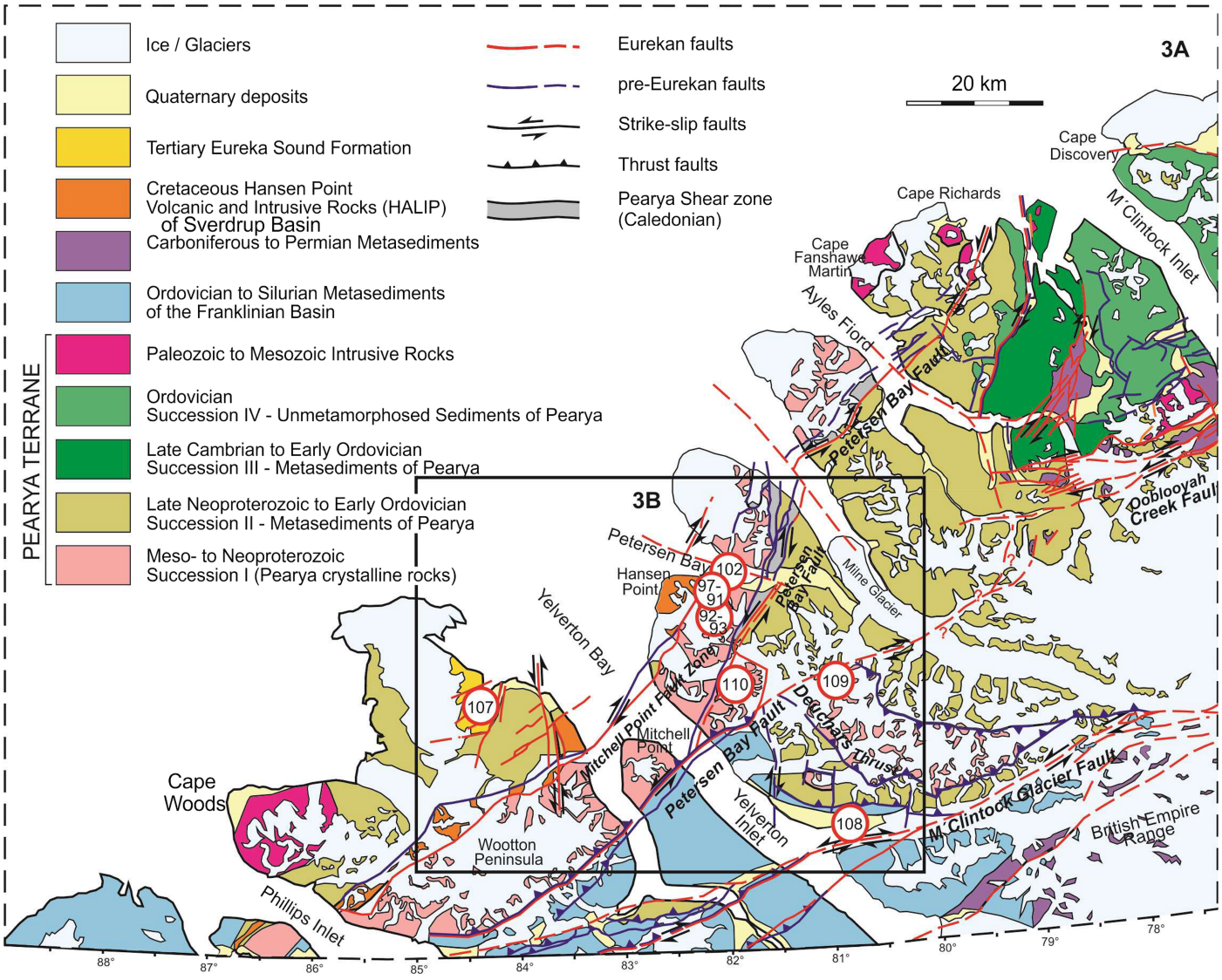

Figure 3. (a and b) Geological maps of the western Pearya terrane (modified after Trettin & Frisch, 1996, Trettin & Mayr, 1996, Estrada et al., 2006, von Gosen et al., 2012, and Piepjohn et al., 2013), including the successions outlined by Trettin (1991). Figure 3a shows the study area and the sampling sites (for simplicity, without the prefixes *C11*). Figure 3b shows close-up of the study area, along with the central AFT ages of the analyzed samples. For the three samples from site C11-107, only the average age of the youngest age group is indicated.

Eureka Sound Group, as patchy exposures of clastic rocks throughout Ellesmere Island. Locally, it reaches a thickness of up to 4 km (Miall, 1986; Ricketts, 1994; Ricketts & Stephenson, 1994). Parts of the Eureka Sound Group are deformed and were thus incorporated into Eurekan deformation.

Pearya is a composite terrane formed of several fault-bound crustal fragments (e.g., Trettin, 1991, 1998). It has been divided into four major tectonostratigraphic successions (Trettin, 1998; see Figure 3a). Succession I is dominated by middle-late Precambrian granitoid orthogneisses with intercalated amphibolites. Successions II and III mainly consist of metamorphosed early-middle Paleozoic sedimentary and igneous rocks (Estrada et al., 2018; Trettin, 1998), whereas the slightly younger, middle Paleozoic sediments of Succession IV are practically unmetamorphosed. So far, no low-temperature thermochronology data have been published from Pearya. AFT and AHe dates from surface exposures of southern and eastern Ellesmere Island are predominantly Paleozoic to Mesozoic (Figure 2), suggesting little exhumation in response to Eurekan deformation (Grist & Zentilli, 2005; Hansen et al., 2011).

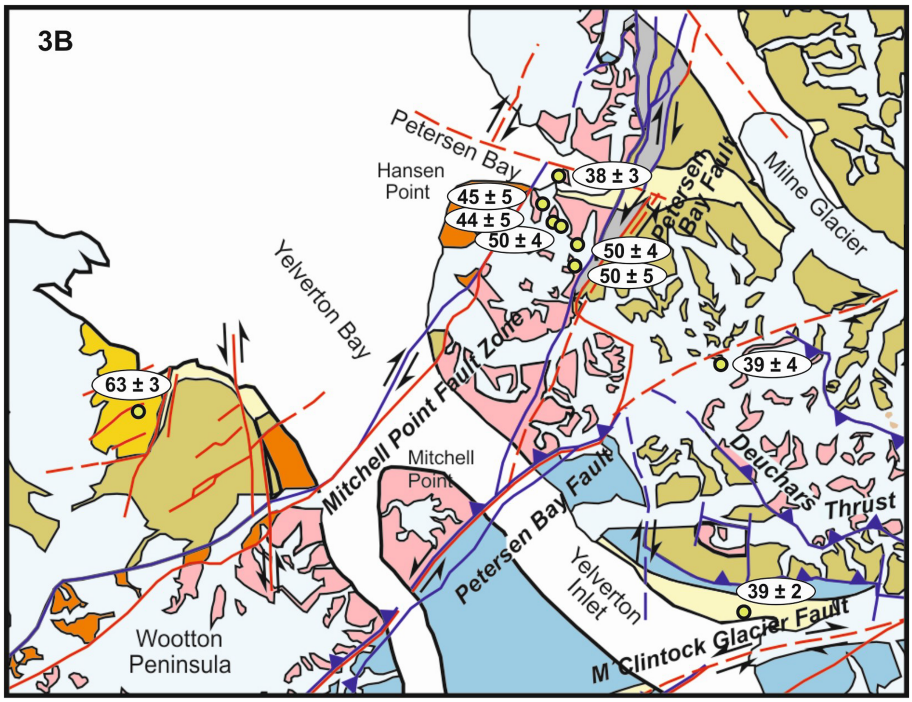

Figure 3. *(continued)*

During the Cretaceous, northern Ellesmere Island was affected by intense intrusive and extrusive mafic to felsic magmatism, including mafic dykes and the Wootton Intrusive and Hansen Point Volcanic complexes, related to the High Arctic Large Igneous Province (e.g., Embry & Osadetz, 1988; Estrada et al., 2016; Ricketts et al., 1985; see Figure 3a). Cretaceous magmatism has been documented in a wide area, including the offshore Alpha Ridge area to the north, and is interpreted to be associated with a mantle plume (Anudu et al., 2016; Embry & Osadetz, 1988; Estrada et al., 1999, 2006; Piepjohn et al., 2013; Ricketts et al., 1985).

Structurally, Pearya is dominated by large strike-slip faults (Figures 2 and 3), mostly orientated parallel to subparallel to the present-day continental margin (Piepjohn et al., 2013, 2016). They show indications for both sinistral and dextral movements. Two prominent shear zones are the Petersen Bay Fault and the M'Clintock Glacier Fault; the latter continues toward the east as Mount Rawlinson Fault. Both the Petersen Bay Fault and the M'Clintock Glacier (Mount Rawlinson) Fault represent the original ductile plate boundary, along which the Pearya terrane was accreted against Laurentia during the Paleozoic Ellesmerian orogeny (Piepjohn et al., 2013). These faults were reactivated as brittle left- and right-lateral strike-slip faults during the Eurekan (Piepjohn et al., 2013; Figure 3), with an unknown amount of vertical displacement. The Petersen Bay Fault and the M'Clintock Glacier Fault are connected, among others, by the E-W striking, south directed Deuchars Thrust, which carried the Pearya rocks of Succession I on top of the metasedimentary rocks of Succession II (Piepjohn et al., 2013; Figure 3b).

2.3. Sedimentary Record and Climate Evolution

Sedimentary deposits that may provide insight into the region's climate evolution during the early Cenozoic are rare. In Pearya, the few occurrences of the Eureka Sound Group are little studied. Their stratigraphy is poorly constrained, but generally, a Late Cretaceous to Paleogene age has been assumed (Estrada et al., 2009; Ricketts & Stephenson, 1994; Trettin, 1991; von Gosen et al., 2012).

As yet, the only scientific deep drilling campaign in the Arctic Ocean took place on top of the Lomonosov Ridge (Arctic Coring Expedition, ACEX, e.g., Stein et al., 2014; Figure 1). The drilled sedimentary section documents the change from subtropical Arctic Ocean temperatures at ~55 Ma (Sluijs et al., 2006) to the occurrence of first, seasonal, sea ice at ~47 Ma (Stickley et al., 2009). One of the arguably most surprising results of ACEX was a substantial hiatus (Backman et al., 2008) or time of very limited deposition (Poirier

Table 1
Information on Analyzed Samples

Sample code	Geological unit	Lithology	Emplacement phase/ deposition age	Location	Longtitude coordinates	Latitude coordinates	Elevation (m)	AFT analysis	MTL meas.	AHe analysis
C11-92	Pearya-Succ. I (basement rocks)	Orthogneiss	Mesoproterozoic / Neoproterozoic (~1,000 – 950 Ma)	S Petersen Bay	82°25.754	81.48.098	1249	√		√
C11-93	Pearya-Succ. I	Amphibolite	— " —	S Petersen Bay	82°25.631	81°48.415	1217			√
C11-91A	Pearya-Succ. I	Orthogneiss	— " —	S Petersen Bay	82°27.446	81°50.354	1000	√	√	√
C11-94A	Pearya-Succ. I	Orthogneiss	— " —	S Petersen Bay	82°27.923	81°53.185	790	√	√	√
C11-95A	Pearya-Succ. I	Orthogneiss	— " —	S Petersen Bay	82°27.940	81°55.862	648	√	√	√
C11-96A	Pearya-Succ. I	Orthogneiss	— " —	S Petersen Bay	82°28.474	82°00.595	540			√
C11-97B	Pearya-Succ. I	Amphibolite	— " —	S Petersen Bay	82°28.829	81°57.933	311	√	√	√
C11-102	Pearya-Succ. I	Orthogneiss	— " —	Island Petersen Bay	82°30.134	81°51.524	47	√	√	√
C11-109B	Pearya-Succ. I	Orthogneiss	— " —	S Petersen Bay	82°21.281	80°54.232	1634	√	√	√
C11-110B	Pearya-Succ. I	Orthogneiss	— " —	S Petersen Bay	82°21.830	81°54.830	449			√
C11-107/2	Eureka Sound Group	Sandstone	Paleocene (~57 Ma)	West of Yelverton Bay	82°20.51	84°26.18	45	√		
C11-107/3	Eureka Sound Group	Sandstone	Paleocene-Eocene (~56 Ma)	West of Yelverton Bay	82°20.50	84°26.17	45	√		
C11-107/5	Eureka Sound Group	Sandstone	Eocene (~54 Ma)	West of Yelverton Bay	82°20.49	84°26.16	45	√		
C11-108	Glacial Outlet	Sand	Quaternary (~2.5–0 Ma)	Yelverton Inlet	82°09.35	80°47.52	4	√	√	√

Note. AFT: apatite fission track, MTL: mean track length, AHe: apatite (U-Th-Sm)/He.

& Hillaire-Marcel, 2011) from ~45 to 18 Ma, which may indicate very shallow water or even exposure of the ridge. Prior to this time, the abundance of freshwater-tolerant species and terrestrial-derived material also indicates shallow-water conditions, at odds with the expected subsidence trend of the Lomonosov Ridge (O'Regan et al., 2008).

Another borehole that has provided important information on the Eocene history of the Arctic is ODP (Ocean Drilling Program) site 913, located in the Norwegian Greenland Sea (Figure 1). The drilled succession contains ice-rafted debris (IRD), which suggests continental glaciation of Arctic land masses already during the middle Eocene (Tripati et al., 2008). IRD occurs particularly frequently at ~40–38 Ma, and ~32–30 Ma (Tripati et al., 2008), and the occurrence of dropstones peaked at ~38 Ma (Eldrett et al., 2007).

3. Materials and Methods

3.1. Sample Material

Sampling took place during the CASE 11 expedition in 2008, organized by the Federal Institute for Geosciences and Natural Resources (Hannover, Germany). Hard rock samples were all collected from Pearya Succession I, which forms an ~10-km-wide exposure along the coast. The samples were taken from different altitudes, covering an elevation range of ~1.6 km (Figure 3 and Table 1). Four of the samples (C11-94 to C11-97) were collected from different nunataks situated adjacent to each other, covering a horizontal distance of ~3 km. The lowest sample (i.e., 47 m above sea level) was collected from a little island (~0.7 km^2) in Petersen Bay (Figure 3a; sample C11-102). The topographically highest sample (i.e., 1,634 m above sea level) is derived from the Deuchars nappe, south of the assumed continuation of the Petersen Bay Fault; that is, it is separated from the other samples by fault(s; Figure 3a; sample C11-109). Several samples were taken from the Eureka Sound Group in Pearya (Figure 3a), assumed to be of Maastrichtian to Paleocene age (Wilson, 1976). It consists of mostly unconsolidated, clastic deposits unconformably overlying Succession II, and it is bound by steep, ENE-WSW dextral strike-slip faults. The sedimentary rocks were folded and thrust-faulted, associated with dextral transpression, indicating that Eurekan tectonics outlasted deposition (Piepjohn et al., 2013). We sampled two ~30-cm thick, dark claystone layers from the central part of the outcrop for palynological analyses. For thermochronological analyses, we sampled weakly lithified sandstone layers below, in between, and directly above the two samples collected for palynological analyses. Finally,

we took a recent sand sample from the frontal outlet of an unnamed glacier, situated along the M´Clintock Glacier Fault (C11-108). We assume that this sample contains material from the glacial valley beneath the ice and from both sides of the M'Clintock Glacier Fault, that is, from the Pearya terrane and from the Franklinian deposits of the former Laurentian margin.

3.2. Methods

Palynological investigations were carried out on two samples (C11-107/4 and C11-107/6) to obtain age constraints for the host sediment and shed light on the depositional environment. Palynological processing followed the protocol of Pross (2001) and included digestion of the original sediment with hydrochloric and hydrofluoric acids, short oxidation with nitric acid, sieving through a 10-mμ mesh, and preparation of strew mounts with glycerine jelly as mounting medium. At least two slides were qualitatively examined for their palynological content, with a special focus on the identification of age-diagnostic dinoflagellate cyst marker taxa.

Thermochronological methods date the passage of a rock through a certain temperature range. Assuming a constant geothermal gradient, cooling paths can be interpreted as reflecting exhumation, triggered either by tectonic denudation or by erosion. Thermal histories involving heating can be interpreted as burial due to tectonic or sedimentary loading. For this study, we applied AFT and (U-Th-Sm)/He (AHe) thermochronology (Dunkl, 2002; Farley, 2000, 2002; Farley et al., 1996; Galbraith & Laslett, 1993; Gleadow, 1981; Hurford & Green, 1993; McDowell et al., 2005). The main temperature sensitivities of these methods are between ~120 and 60 °C and 85 and 40 °C, respectively (Wagner et al., 1989; Wolf et al., 1998). Thus, the combination of both methods allows monitoring geodynamic processes of the upper 4 to ~1 km of the Earth's crust, assuming a geothermal gradient of ~30 °C/Ma. AFT and AHe data can be integrated using thermal history modeling. For this, track length shortening and He diffusion in apatite are described by algorithms that are derived from laboratory experiments and calibrated by benchmark studies for extrapolation to geological time scales (Ketcham, 2005). Thermal histories are extracted from the data by inverse modeling using a Monte Carlo approach, comparing the predicted data with the data actually observed (Ketcham, 2005; Ketcham et al., 2007a, 2007b, 2011; Ketcham et al., 2015).

For sedimentary samples, which were not heated to temperatures above the closure temperatures of the AFT system after their deposition, AFT dates record the cooling and exhumation history of the sediment source area. AFT ages of single grains are statistically grouped in different populations using the binomial peak fitting method (Brandon, 2007). The lag time, which is the time between isotopic closure of the AFT system and sediment deposition of the sample, is also calculated for each defined AFT age group. Thermal modeling on detrital samples is only performed when the samples have been thermally reset postdeposition or show a single AFT age group, because otherwise, the measured track lengths data cannot be clearly assigned to the corresponding AFT age group. Details on the analytical procedures and thermal history inversions are described in the Supporting Information (SI) file.

4. Results and Interpretation

4.1. Age Assignment and Depositional Environment of Samples From the Eureka Sound Group (C11-107/4 and C11-107/6)

Palynological analysis showed that both samples are overwhelmingly dominated by plant debris and amorphous organic matter but also contain pollen and spores, as well as marine dinoflagellate cysts; single foraminifer test linings also occur. Palynomorph preservation is generally moderate to poor.

Sample C11-107/4: Based on the occurrence of the dinoflagellate cyst *Cerodinium wardenense* (and neglecting the possibility of reworking), the sample has a latest Paleocene to early Eocene age. Available data suggest that *Cerodinium wardenense* has a first occurrence datum of ca 57 Ma (Williams et al., 2004; all ages based on Gradstein et al., 2012); its last occurrence datum is at ca 54.2 Ma (Williams et al., 2004), its last common occurrence at ca 55.5 Ma (Bujak & Mudge, 1994). If the specimens of *Cerodinium wardenense* are accepted as reworked, the given age would be a maximum age.

Sample C11-107/6: Age-diagnostic dinoflagellate cysts in this sample comprise *Cerodinium wardenense* and *Wetzeliella astra*. They indicate an early Eocene age. *Wetzeliella astra* has a first occurrence date of 54 Ma in

Table 2a
Binomial Peak Fitting of Samples from the Eureka Sound Group

Sample	deposition	AFT age	n1 / %	AFT age	n2 / %	AFT age	n3 / %	lag time	integrated	D.R.	D.R.
Code	**age**	**group 1**		**group 2**		**group 3**		**group 1**	**cooling rate**	**(20 °C/km)**	**(40 °C/km)**
C11-107/5	~54 Ma	64 ± 3 Ma	76 / 85%	127 ± 6 Ma	9 / 10%	364 ± 10 Ma	4 / 5%	10 Myr	10 °C/Myr	0.5 km/Myr	0.25 km/Myr
C11-107/3	~56 Ma	63 ± 7 Ma	30 / 78%	133 ± 17 Ma	8 / 20%	321 ± 19 Ma	1 / 2%	7 Myr	14 °C/Myr	0.7 km/Myr	0.35 km/Myr
C11-107/2	~57 Ma	63 ± 3 Ma	77 / 76%	223 ± 12 Ma	24 / 24%	-	-	6 Myr	17 °C/Myr	0.85 km/Myr	0.43 km/Myr
C11-107/2-3-5 merged	~55.5 ± 1.5 Ma	63 ± 3 Ma	180 / 79%	129 ± 6 Ma	25 / 11%	266 ± 9 Ma	24 / 10%	7.5 Myr	13 °C/Myr	0.65 km/Myr	0.33 km/Myr

Note. nx / %: number and percentage of grains contained in age group x; *D.R.:* integrated denudation rates for geothermal gradients of 20 and 40 °C/km. Cooling and denudation rates only refer to AFT age group 1. The single-grain ages were calculated using zeta calibration method (Hurford & Green, 1983), glass dosimeter CN-5 and zeta value of 328.42 ± 16.76 year/cm2 (A. Vamvaka).

Siberia (Frieling et al., 2014). As outlined above, *Cerodinium wardenense* has a first occurrence date of ca 57 Ma and a last occurrence date at ca 54.2 Ma (Williams et al., 2004).

From a climatostratigraphic perspective, the pollen assemblages in both samples are fully compatible with a Paleocene to early Eocene age. The assemblages comprise *Taxodium* (swamp cypress), *Tilia* (linden), and *Carya* (hickory), which are indicative of a warm, humid climate as it is well known to have prevailed in the high northern latitudes at that time (e.g., Sluijs et al., 2006).

Previously, the deposits were characterized as of late Maastrichtian to Paleocene age. Since the two samples were collected from the central part of the outcrop, we cannot exclude that the oldest strata at the basis of the outcrop were indeed deposited during the Cretaceous. However, our data also show that the middle to upper part of the sediments are at least of early Eocene age, and accordingly, deposition of the Eureka Sound Group on Pearya lasted longer than previously assumed.

For both samples, the identified dinoflagellate cysts in combination with the pollen and spore assemblages and the high abundance of plant debris imply a proximal, marginally marine setting, similar to coastal swamp environments today encountered in the southeastern United States. Unequivocal evidence for marine conditions also comes from the finding of (few) foraminifer test linings.

4.2. Thermochronology and Thermal History Modeling

AFT age groups contained in the sediments of the Eureka Sound Group are remarkably consistent, with a dominant Paleocene age group (~63 ± 3 Ma; 79% of grains; Table 2a). The two upper sedimentary samples also contain an Early Cretaceous age group (~128 ± 6 Ma) and a weakly constrained Devonian-Carboniferous age group (~360 ± 9 Ma), while the lowest sample contained a Triassic age group (~223 ± 12 Ma). The different, pre-Paleocene age groups contained in the three samples (i.e., Early Cretaceous, Triassic, and Carboniferous) may indicate different source areas of the sediments through time. However, the small number of AFT single-grain ages that can be classified into pre-Paleocene age groups, as well as the big age range they cover (i.e., from ~75 to >500 Ma), precludes reliable identification of older age groups. Nevertheless, there is clear indication for the existence of at least a Cretaceous and a pre-Cretaceous age group.

The Paleocene age groups contained in Paleocene to Early Eocene sediments imply rapid cooling of the source area: The lag time (see section 3.2 for definition) ranges between 6 and 10 Myr (Table 2a and figures in SI file), suggesting time-integrated cooling rates between ~17 and 10 °C/Myr. Assuming geothermal gradients between 20 and 40 °C/km, average denudation rates for the lag time can be estimated between 0.85 and 0.25 km/Myr. Since denudation was presumably related to crustal extension/transtension (Harrison, 2006; Anudu et al., 2016; Gion et al., 2017; see also discussion on the pre-Eurekan evolution), we consider a higher geothermal gradient to be more realistic and thus estimate denudation rates of ~0.45 to 0.25 km/Myr for the Paleocene, pre-Eurekan stage, that is, for the time between isotopic closure (~63 Ma) and sediment deposition (~56 Ma). The increasing lag time and decreasing cooling rates from early to late Paleocene argue for an episodic high exhumation pulse during the Early Paleocene.

Table 2b
Results of AFT Analysis From the Pearya Basement and Recent River Sand

Sample	Lithology	Elevation (m)	n	ρ_s	N_s	ρ_i	N_i	ρ_d	N_d	$P(\chi^2)$ (%)	D	Central age ± 1σ (Ma)	MTL ± s.d. (μm)	NMT length measur.	Dpar ± S. D. (μm)	U (ppm)
C11-109B	Orthogneiss	1,634	20	3.21	170	27.81	1474	20.40	33,127	100.0	0.00	**39 ± 4**	**14.31 ± 1.16**	55	1.65 ± 0.15	15.5
C11-92	Orthogneiss	1,249	21	3.61	137	25.14	955	21.40	33,127	100.0	0.00	**50 ± 5**	**n.a.**	n.a.	1.56 ± 0.12	15.3
C11-91A	Orthogneiss	1,000	20	5.49	284	39.07	2022	21.69	33,127	98.5	0.00	**50 ± 4**	**13.92 ± 1.19**	77	1.49 ± 0.10	22.8
C11-94A	Orthogneiss	790	31	4.16	332	29.16	2325	21.26	33,127	100.0	0.00	**50 ± 4**	**14.45 ± 1.06**	88	1.45 ± 0.13	17.0
C11-95A	Orthogneiss	648	22	5.11	135	40.38	1067	21.12	33,127	100.0	0.00	**44 ± 5**	**14.01 ± 1.51**	61	1.53 ± 0.13	25.9
C11-97B	Amphibolite	311	21	7.51	142	59.67	1129	21.97	33,127	100.0	0.00	**45 ± 5**	**14.59 ± 1.22**	81	1.62 ± 0.16	29.9
C11-102	Orthogneiss	47	21	10.2	337	90.66	2991	20.83	33,127	98.7	0.00	**38 ± 3**	**14.20 ± 1.79**	87	1.81 ± 0.18	51.0
C11-108	Recent Sand	4	93	4.16	791	36.32	6912	20.54	33,127	100.0	0.00	**39 ± 2**	**14.25 ± 1.31**	71	1.50 ± 0.12	25.2

Note. n: number of counted grains; $\rho s/\rho i$: spontaneous/induced track densities. All densities are given as 10^5 tracks cm^{-2}; Ns/Ni: number of spontaneous/induced tracks; ρd: dosimeter track density ; Nd: number of tracks counted in dosimeter; $P(\chi^2)$: probability of obtaining chi-square value (χ^2) for n degree of freedom (where n is the number of crystals minus 1); D: Dispersion; MTL: mean horizontal confined track length without c-axis projection; S.D.: Standard Deviation; NMT: number of measured confined track lengths; Dpar: mean etch pit diameter of fission tracks; U: Mean Uranium content of apatite. The ages were calculated using zeta calibration method (Hurford & Green, 1983), glass dosimeter CN-5 and zeta value of 328.42 ± 16.76 year/cm^2 (A. Vamvaka).

AFT dates from the basement samples range from 50 ± 5 to 38 ± 3 Ma and AHe dates from 56 ± 6 to 9 ± 0.8 Ma (Tables 2b and 3 and Figures 3b and 4). Overall, the modeled thermal histories show that cooling and thus exhumation related to the Eurekan (and post-Eurekan) deformation was episodic, with three distinct periods of rapid cooling at about ≥55 to 48 Ma (referred to as *Eureka Stage 1* in the following), 44 to 38 Ma (referred to as *Eurekan Stage 2* in the following), and 34 to 26 Ma (referred to as post-Eurekan Stage), and periods of slower cooling in between (Figure 5). For the samples collected between 47 and 1,000 m above sea level, that is, from basement exposures undisturbed by large fault zones, the models follow the expected trend: The older cooling periods are best recorded in the highest samples, whereas the younger cooling history is recorded by the lower samples. The 55 to 48 Ma Stage 1 cooling period is best defined by sample C11-91A, which documents cooling from >120 to ~60 °C during this time. Assuming a typical orogenic *Barrow-type* geothermal gradient of 20 to 30 °C, this can be transformed into net exhumation of 2 to 3 km.

The ~44 to 38 Ma cooling period of Stage 2 is best recorded by the samples from the middle part of the sampled section (Figure 5). From the time-temperature paths, about 50 °C of net cooling during this time can be derived, which can be transformed into net exhumation of 2 to 3 km. Presumably, this exhumation period was coeval with dextral strike-slip faulting, which truncated and deformed the sediments of the Eureka Sound Group. For the same period, even higher net exhumation, of ~3 to >4 km (i.e., cooling of ~80 °C), is shown farther south, by the thermal history of the highest basement sample (C11-109B, 1,634 m; Figures 3–5). This sample deviates from the trend observed from the other samples, in that it does not record the earliest Eocene Stage 1 cooling period, as it would be expected from its present-day altitude, but rather, it records the Stage 2, 44 to 38 Ma, cooling period.

Finally, the last, post-Eurekan stage of rapid cooling took place between ~34 and 26 Ma, and it is best recorded by the lowermost samples. Net cooling during this period was approximately 80 °C, equivalent to ~3 to 4 km of net exhumation. Summing up, our models suggest net exhumation of 8 to 11 km for the Eurekan and post-Eurekan stages, in agreement with field observations that deformation is predominantly brittle and that no significant metamorphism was associated with the Eurekan orogeny, and also in agreement with previous geochronological data from Pearya, which show that the $^{40}Ar/^{39}Ar$ system particularly in biotite was disturbed by the post-Ellesmerian evolution, but did not experience a full resetting in response to Eurekan tectonics (Estrada et al., 2018).

The recent glacial sand draining the M'Clintock Glacier Fault (C11-108) contains a tight age distribution (χ^2 probability of 100%; Table 2b), something rather unusual for a detrital sample. However, since the results point out only one dominant age group (i.e., both 100% χ^2 probability), we therefore combined its AFT dates with track lengths measurements and with detrital AHe dates from the same sample in our thermal history inversions. The AHe dates showed two main age groups, one of ~31 Ma, and one of ~11 Ma (Table 3), but

Tectonics

10.1029/2019TC005621

Table 3
Results of (U-Th-Sm)/He Thermochronology

Sample code location/ elevation	Aliquot	Lithology	Raw age (Ma)	Error (Ma)	Ft weighted	Corrected age (Ma)	Error (%)	Error (Ma)	Mass (μg)	^{147}Sm (ppm)	^{232}Th (ppm)	^{238} + ^{235}U (ppm)	^{4}He (ncc)	eU (ppm)	r-sphere (μm)	Mean age (Ma)	S.E. (Ma)	S.D. (Ma)
C11-109B	1	Orthogneiss	33.8	0.2	0.8	44.6	0.6	0.3	2.6242	50.5	3.88	24.4	0.2759	25.58	66	**44.6**	0.3	
S Peterson Bay	2		*55.8*	0.5	0.8	*74.0*	0.8	0.6	2.4526	35.8	0.953	7.38	0.1311	7.80	65			
1634 m	3		16.5	1.0	0.7	25.0	2.0	0.5	0.4473	36.7	10.8	22.8	0.0740	25.57	49			
C11-92	1	Orthogneiss	*81.9*	1.5	0.7	*91.4*	1.8	1.6	2.0781	2.86	2.82	1.73	0.0501	2.41	60	**45.4**	1.0	7.04
S Peterson Bay	2		42.1	1.3	0.7	46.8	3.0	1.4	1.6441	3.10	2.37	2.04	0.0220	2.61	56			
1249 m	3		33.5	0.9	0.7	33.5	2.6	0.9	3.3552	1.92	0.179	0.894	0.0130	0.95	64			
	4		35.4	0.4	0.8	44.1	1.2	0.5	2.4757	4.10	6.74	5.11	0.0716	6.72	65			
C11-93	1	Amphibolite	*99.2*	6.1	0.6	*169.0*	6.3	10.7	0.0005	3.16	2.05	0.774	0.0080	1.27	39			
S Peterson Bay	2		*210.1*	13.0	0.6	*343.7*	129.4	444.8	0.0012	0.128	0.000	0.171	0.0052	0.17	41			
1217 m	3		*184.9*	11.5	0.6	*313.1*	23.4	73.2	0.0010	0.429	0.000	0.148	0.0035	0.15	39			
C11-91A	1	Orthogneiss	34.3	0.3	0.7	48.5	0.9	0.4	1.2748	63.3	18.3	24.4	0.1547	29.01	54	**48.4**	0.5	1.51
S Peterson Bay	2		*52.9*	0.6	0.8	*69.8*	1.1	0.8	2.9703	27.9	7.13	6.19	0.1517	8.02	67			
1000 m	3		31.0	0.3	0.6	49.9	1.1	0.5	1.2886	39.1	10.3	11.0	0.0664	13.61	42			
	4		30.5	0.4	0.6	46.9	1.2	0.6	1.0079	43.5	19.5	14.3	0.0717	19.12	46			
C11-94A	1	Orthogneiss	32.2	0.3	0.7	46.7	0.8	0.4	1.9145	68.0	15.7	31.6	0.2677	35.67	52	**47.0**	0.4	3.12
S Peterson Bay	2		36.3	0.3	0.7	50.3	0.8	0.4	3.6994	59.8	10.9	18.2	0.3454	21.08	58			
790 m	3		*45.5*	0.4	0.7	*64.3*	0.8	0.5	2.8142	34.5	6.25	8.26	0.1119	9.92	54			
	4		12.0	0.0	0.7	17.4	0.4	0.1	2.7205	74.3	21.0	33.8	0.5045	39.12	52			
	5		28.7	0.2	0.7	44.1	0.8	0.4	1.7592	52.0	19.4	20.5	0.1557	25.31	46			
C11-95A	1	Orthogneiss	*503.8*	15.2	0.6	*776.8*	3.0	23.3	0.7975	0.912	1.43	2.82	0.1607	3.16	45	**41.2**	2.8	4.54
S Peterson Bay	2		*110.7*	1.0	0.8	*145.0*	0.9	1.3	2.4473	5.17	5.34	16.2	0.5768	17.44	67			
638 m	3		30.9	0.4	0.8	40.6	1.5	0.6	2.3611	4.90	3.77	13.7	0.1297	14.65	67			
	4		24.4	0.5	0.7	35.1	1.9	0.7	2.4540	2.75	2.89	5.83	0.0474	6.52	52			
	5		28.1	6.9	0.7	42.8	24.6	10.5	1.6209	1.61	0.104	3.49	0.0194	3.52	46			
	6		35.6	0.0	0.7	47.6	2.4	1.1	0.0037	18.6	9.40	6.55	0.1420	9.74	54			
	7		31.6	2.0	0.8	39.9	3.2	1.3	0.0066	1.44	2.07	2.53	0.0770	3.09	67			
C11-96AI	1	Orthogneiss	27.86	1.73	0.7	41.8	0.6	0.2	0.0014	82.4	22.3	47.6	0.0014	53.31	48	**42.4**	0.3	1.07
S Peterson Bay	2		29.70	1.84	0.7	43.7	0.8	0.3	0.0021	87.7	14.4	29.8	0.0021	33.67	50			
540 m	3		26.82	1.66	0.6	41.8	0.6	0.3	0.0015	171	44.6	89.8	0.0015	101.19	44			
	4		34.10	2.11	0.6	52.6	1.2	0.7	0.0009	109	9.15	19.7	0.0009	22.48	45			
C11-97B	1	Amphibolite	22.6	8.1	0.7	33.5	35.7	12.0	1.3905	0.922	0.000	0.144	0.0006	0.15	49	**34.9**	4.2	10.45
S Peterson Bay	2		26.2	4.9	0.8	34.3	18.5	6.4	2.1928	0.397	0.015	0.160	0.0012	0.17	67			
311 m	3		*129.4*	100.3	0.7	*194.8*	77.5	151.0	1.0930	0.343	0.000	0.046	0.0008	0.05	47			
	4		15.0	0.4	0.6	23.6	2.5	0.6	1.3960	1.21	0.029	4.08	0.0104	4.10	43			
	5		33.2	0.9	0.6	52.0	2.8	1.5	1.5915	1.22	0.153	3.58	0.0232	3.62	44			
	6		21.0	1.3	0.7	31.1	2.5	0.8	1.3514	4.09	3.57	5.24	0.0210	6.10	50			
C11-102I	1	Orthogneiss	27.4	1.7	0.7	40.4	3.2	1.3	1.9227	9.00	7.18	24.4	0.1670	26.17	54	**44.1**	1.6	3.39
Island	2		31.5	2.0	0.8	41.9	3.3	1.4	4.5648	10.6	10.9	28.2	0.5380	30.87	45			
Peterson Bay	3		24.8	1.5	0.6	41.7	3.3	1.4	0.6910	6.94	12.6	15.8	0.0390	18.78	47			
47 m	4		29.6	1.8	0.6	49.7	4.0	2.0	0.6910	9.16	25.1	26.3	0.0800	32.23	40			
	5		29.6	1.8	0.7	45.0	3.6	1.6	1.5773	6.08	15.6	16.3	0.1130	19.98	39			
	6		29.7	1.8	0.6	47.4	3.8	1.8	1.1183	6.12	10.3	11.7	0.0570	14.14	63			
	7		30.6	1.9	0.7	42.9	3.4	1.5	2.9925	9.09	11.0	20.1	0.2530	22.78	49			

Table 3
(continued)

Sample code location/ elevation	Aliquot	Lithology	Raw age (Ma)	Error (Ma)	Ft weighted	Corrected age (Ma)	Error (%)	Error (Ma)	Mass (µg)	^{147}Sm (ppm)	^{232}Th (ppm)	^{238} + ^{235}U (ppm)	^{4}He (ncc)	eU (ppm)	r-sphere (µm)	Mean age (Ma)	S.E. (Ma)	S.D. (Ma)
C11-108	1	Recent Sand	24.8	1.5	0.7	33.2	2.6	0.9	4.5860	98.1	79.1	66.9	0.1990	86.03	56	**31.5**	0.8	2.37
Yelverton Inlet	2		21.6	1.3	0.7	29.8	2.4	0.7	1.7124	163	2.67	8.29	0.3000	9.81	47			
4 m	3		7.1	0.1	0.8	9.0	0.8	0.1	0.0036	73.2	29.8	103	0.3363	110.85	73	**11.2**	0.1	2.07
	4		8.6	0.1	0.8	11.3	0.8	0.1	0.0047	28.6	30.8	48.2	0.2719	55.59	65			
	5		9.3	0.1	0.7	13.2	0.9	0.1	0.0029	65.0	18.9	63.0	0.2249	67.83	55			
	6		*542.2*	4.6	0.6	*917.3*	1.1	10.5	0.0011	62.6	44.7	7.91	1.4354	18.75	40			
C11-110B	1	Orthogneiss	37.6	0.8	0.7	56.1	5.7	3.2	0.8693	1.66	5.36	9.20	0.0416	10.47	48	**50.8**	2.7	7.52
S Peterson Bay	2		*41.2*	0.4	0.6	*64.0*	6.4	4.1	1.4274	9.77	9.64	20.0	0.1589	22.28	44			
449 m	3		27.7	0.4	0.6	45.5	4.6	2.1	0.9615	0.814	6.09	12.5	0.0451	13.97	43			
	4		*55.2*	0.5	0.7	*84.1*	8.4	7.1	0.8219	22.9	29.9	38.0	0.2494	45.17	46			

Note. FT: Factor used for alpha-ejection correction, *eU*: effective Uranium content calculated as "^{238} + ^{235}U+(0.235*^{232}Th) + (0.0055*^{147}Sm)"; *r-sphere*: equivalent sphere radius; *SE*: standard error, *SD*: standard deviation; *text in Italics*: presumably containing inclusions apatites; *underlined (red) text*: aliquots used in modeling.

only the first group could be combined with the AFT dates in modeling (i.e., providing good paths; see also chapter S2 of the SI file for analytical description regarding thermal modeling and used terminology). The resulting time-temperature history is similar to the one derived from the deepest incised areas of the basement section, reflecting Stage 2 and post-Eurekan rapid cooling from ~44 to 38 Ma and from 34 to 26 Ma, and the period of slow cooling in between (Figure 5). If this sample originates from the entire glacial catchment including both sides of the M'Clintock Fault Zone, it implies that pronounced Eurekan erosion is not restricted to the coastal basement exposure but has affected larger areas of northern Ellesmere Island, including the Franklinian Basin south of the Pearya terrane boundary.

The difference in the net exhumation in the northern and southern parts of the study area may be explained by different timing and different levels of activity of the main fault zones (or segments of the same fault zone) during each exhumation period. It seems that the northeastern prolongation of Petersen Bay Fault and/or Mitchell Point Fault zone has experienced maximum activity during Eureka Stage 1 and the pre-Eurekan period of rapid cooling (i.e., ~55 to 48 Ma and ~34 to 26 Ma), as supported by the exhumation shown by the thermal histories of the samples C11-91A to C11-102 (Figures 3 and 5). The exhumation at the C11-109b sample site is most probably connected to the activity of the southern segment of Petersen Bay fault (or even possibly of the Deuchars Thrust (?)), which should be significant at least during the Eureka Stage 2 exhumation period, as supported by our data. Intense fault activity may also account for the site's present much higher altitude (i.e., 1,634 m), compared to that of samples C11-94A and C11-95 (i.e., 790 and 648 m; meaning ~1-km vertical difference). The thermal history of the samples from both sides of the southern segment of Petersen Bay fault (i.e., C11-109B versus C11-94A and C11-95) shows that they were at the same crustal depth (~60 °C; see Figure 5) at ~40 Ma. Finally, the thermal history of sample C11-108 implies an activation of M'Clintock Glacier Fault zone in the south at least during Eureka Stage 2 and the post-Eurekan cooling periods (i.e., ~44 to 38 Ma and 34 to 26 Ma). In conclusion, our data support the argument of Piepjohn et al. (2013) that all these originally Ellesmerian structures were actively involved in the Eurekan orogeny. We suggest that they were responsible for increased localized exhumation, which is in accordance with the expected result caused by strike-slip structures (such as by localized transpression along restraining bends or at the flanks of developed flower structures).

5. Discussion

5.1. Comparison With Other Arctic Areas Deformed During the Eurekan

Previous studies from Ellesmere Island show some relatively clear trends: The cratonic areas and most of the Franklinian sediments exposed in southern and eastern Ellesmere Island are characterized by Mesozoic or even Palaeozoic AFT and AHe dates (Grist & Zentilli, 2005; Hansen et al., 2011; Figure 2), indicating that erosion during the Cenozoic was not sufficient to expose ages reflecting Eurekan exhumation; that is, Eurekan and post-Eurekan denudation was limited to <2 to 3 km (the required depth to fully reset the AHe system). Thus, in south(east) Ellesmere Island, Eurekan deformation was not associated with significant exhumation. AFT data from the Sverdrup Basin exposed in western Ellesmere Island and on adjacent Axel Heiberg Island yield a mixed signature: Some of the surface exposures revealed similar old ages as the southeastern areas, but (pre/-)Eurekan, Paleogene AFT dates were also observed, predominantly in the vicinity of large fault systems (Arne et al., 1998; Arne et al., 2002). Studies on well samples showed that the Eurekan age signal mostly occurs at depth of 1 to 2 km below the surface (Arne et al., 2002). Modeling of combined AFT and vitrinite reflectance data from the Sverdrup Basin yielded predominantly Paleocene, pre-Eurekan cooling (Arne et al., 2002). Thus, it seems that Eurekan exhumation was

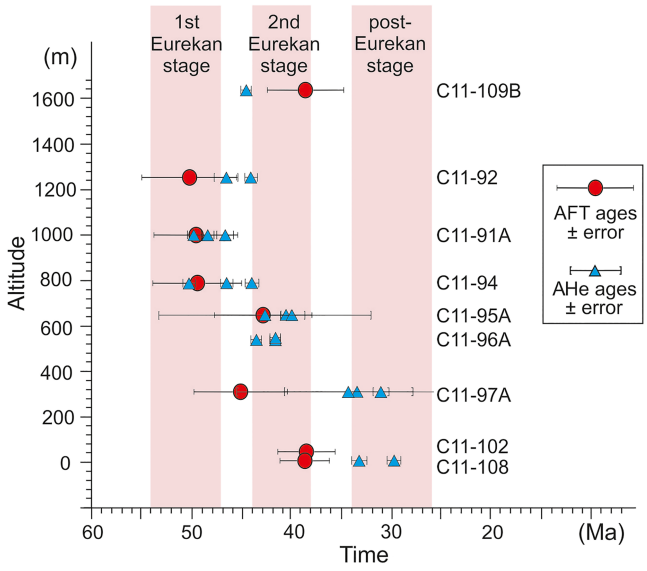

Figure 4. AFT and AHe age-elevation profile of the analyzed samples (see also Figure 3 and Tables 1 and 2). Only the AHe ages used for modeling are depicted here. Also shown are samples C11-92 and C11-96A for which no model was produced and no AFT date was calculated, respectively. Some AHe dates could not be integrated with the corresponding AFT date through thermal history modeling. These AHe dates are documented in Table 3. The pink bars illustrate the redefined stages of Eurekan and post-Eurekan evolution, as derived from our thermochronology data.

mostly focused along the northern margin of Ellesmere Island and it seems that the younger, Eocene to Oligocene exhumation periods are exclusively recorded in the north. It should be noted, however, that previous studies used different modeling approaches and annealing algorithms than our study and are thus not fully comparable. Furthermore, low-temperature thermochronology data coverage particularly of the interior of Ellesmere Island is still sparse, and so the detailed exhumation patterns are still unknown.

In Greenland, the Eurekan belt comprises the northern and northeastern margins. No low-temperature thermochronology data exist so far from that area. In North Greenland, $^{40}Ar/^{39}Ar$ dates indicate thermal resetting between 49 and 47 Ma (Tegner et al., 2011), coinciding with rapid exhumation in Pearya. For northeast Greenland, both Late Cretaceous to earliest Paleocene deformation (Håkansson & Pedersen, 2001; Lyberis & Manby, 2001) and Eocene deformation (Tegner et al., 2011; von Gosen & Piepjohn, 2003) were suggested, but the existing data coverage does not allow a direct comparison to Ellesmere Island.

In Svalbard, data from the Central Tertiary Basin showed that rapid subsidence and maximum burial occurred between ~55 and 50 Ma, followed by basin inversion and rapid erosion between ~50 and 40 Ma (Dörr et al., 2019; Figure 6). Both periods match rapid exhumation in Pearya. Furthermore, a distinct cooling period between ~35 and 25 Ma associated with ~2 to 3 km of exhumation was reported for West Svalbard by Blythe and Kleinspehn (1998), again very similar to our findings from Pearya (Figure 6). Together, the thermochronology data from Pearya and Svalbard suggest a surprisingly synchronous behavior along the >2,000-km-long Eurekan belt, although, of course, the generally low data coverage needs to be kept in mind.

5.2. Relationship to Plate Tectonics

5.2.1. Pre-Eurekan Evolution of Pearya

None of the investigated, present-day exposures of Pearya still record the pre-Eurekan evolution in their low-temperature systems. Information on the pre-Eurekan, however, is stored in the sedimentary deposits of the Eureka Sound Group (Table 2a). The weakly constrained pre-Cretaceous age groups (i.e., the Carboniferous age group of the two younger samples and the Triassic age group traced in the older sample) may all reflect cooling after the Ellesmerian orogeny and formation of the Sverdrup basin. The ~130-Ma age group is most likely related to extensional tectonics and crustal thinning associated with opening of the Amerasia Basin.

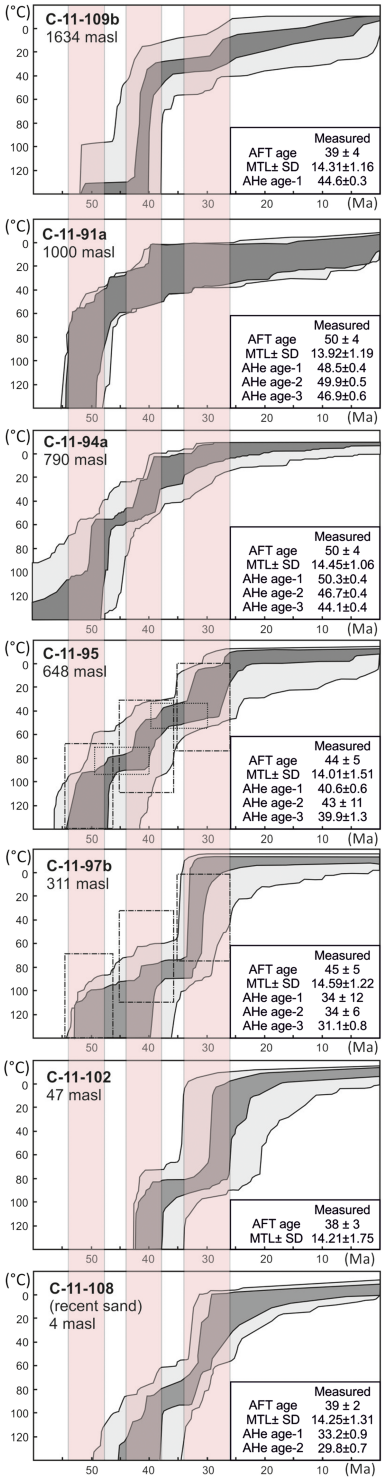

Figure 5. Modeled thermal histories extracted from the AFT and AHe dates reported in Tables 2 and 3. Six of the modeled samples are derived from different altitudes of basement rock exposures. Sample C11-108, by contrast, is derived from recent river deposits (see also Figure 3, as well as Tables 1 and 3; the AHe aliquots used for modeling are underlined in Table 3). The dark gray envelope includes all statistically good paths, the light gray envelope includes those with acceptable fits (with *good* defined as a goodness-of-fit value ≥0.5, and acceptable as a goodness-of-fit value ≥0.05, based on the comparison of the measured input data and modeled output data). The pink shading highlights periods of enhanced exhumation. The observed central AFT age (in Ma), measured mean track length without c-axis projection (MTL, in μm), standard deviation (SD, in μm), and the AHe ages (Ma) used for modeling are provided.

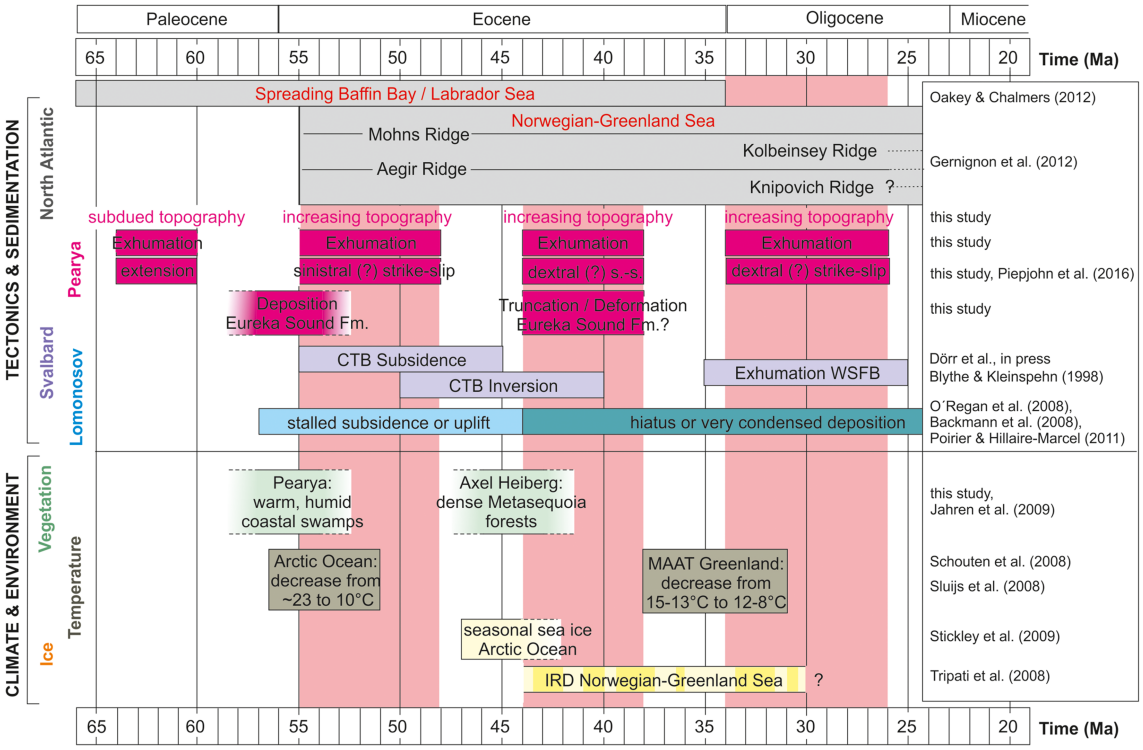

Figure 6. Temporal relationships between tectonics, sedimentation, and environmental change in parts of the Arctic. CTB: Central Tertiary Basin; MAAT: mean annual air temperature; WSFB: West Spitsbergen Foldbelt. Dark yellow color refers to periods of enhanced IRD (ice-rafted debris) accumulation rates in the Norwegian-Greenland Sea, defined by us as >5 mg · cm^3 · kyr, using the data of Tripati et al. (2008). The pink shading indicates the periods of enhanced exhumation, as derived from the thermochronology data.

Our data thus corroborate previous assumptions of an Early Cretaceous onset of formation of the Amerasia Basin.

Finally, the Paleocene age group indicates a rapid exhumation pulse at a rate of ≥0.4 km/Myr prior to sediment deposition. We interpret this rapid exhumation as reflecting a generally extensional period related to crustal thinning and tectonic denudation rather than tectonic uplift, because (i) it is coeval with basin formation and deposition in a coastal marine environment (as indicated by the palynology data) and, thus, with subsidence of parts of the continental margin, and (ii) it coincides with a period of crustal extension from Late Cretaceous-Cenozoic times proposed by interpretation of aeromagnetic and gravity data for the northeastern Canadian Arctic margin (Anudu et al., 2016) and also predicted between 63 and 55 Ma by GPlates modeling (Gion et al., 2017; Harrison, 2006). Crustal thinning may have caused transtensional reactivation of preexisting fault zones, locally leading to pull-apart(?) basin(s) formation. The depressed areas became sites of sediment deposition, sourced from the eroding tectonically uplifted edges. The eroding source area of the basin fillings may theoretically also be part of relict topography associated with rift shoulder uplift during Mesozoic opening of the Amerasia Basin (e.g., Alvey et al., 2008; Tailleur, 1973).

The extensional (transtensional) phase in Pearya and localized subsidence ended during the early Eocene and gave way to (trans)pression. This is in agreement with a deposition age of ~54 Ma obtained from the youngest sedimentary rocks sampled from the Eureka Sound Group. The change of the deformational regime was triggered by the onset of spreading in the Norwegian-Greenland Sea and the associated onset of independent movements of the Greenland plate. This caused deformation and erosion of the Paleocene-Eocene sedimentary deposits of Pearya and led to renewed rapid exhumation of the continental margin, now related to tectonic uplift and the onset of the Eurekan orogeny.

5.2.2. Eurekan and Post-Eurekan Evolution

Thermochronology data of the basement exposures revealed three periods of enhanced exhumation, at 55–48 Ma, 44–38 Ma, and 34–26 Ma. As recognized by previous studies, Eurekan deformation results from

movements of the Greenland plate, which in turn are driven by seafloor spreading in the Baffin Bay/Labrador Sea and the Norwegian-Greenland Sea. In the following, we attempt to correlate our refined temporal framework of Eurekan exhumation of Pearya with changes of the spreading regime in the North Atlantic.

The first period of rapid exhumation is nearly identical with the timing of Eurekan Stage 1 as previously defined by Piepjohn et al. (2016; i.e., 53–47 Ma), thus providing strong independent support for the timing of early Eurekan deformation. Early Eurekan exhumation of Pearya coincides with *Oceanic Phase 1* of the Norwegian-Greenland Sea (Gernigon et al., 2012), which was characterized by simultaneous onset of spreading at relatively high rates along the Aegir and Mohns Ridges (Mosar et al., 2002; Gaina et al., 2009; Figure 7 a). Spreading of the Labrador Sea/Baffin Bay was ongoing, but with a distinct change of spreading directions, as compared to the Paleocene spreading regime (Oakey & Chalmers, 2012). The DeGeer Fracture Zone was active and accommodated transpressive movements between Svalbard and Northeast Greenland, resulting in deformation along the West Spitsbergen margin (Piepjohn et al., 2016) and associated subsidence of the Central Tertiary Basin (Dörr et al., 2019; Jones et al., 2017). Because Pearya experienced rapid exhumation at the same time and of about the same order of magnitude as the West Spitsbergen Foldbelt (whereas the rest of Ellesmere Island has experienced less intense Eurekan exhumation), and because Pearya is dominated by strike-slip tectonics (whereas the rest of Ellesmere Island also shows Eurekan compressional structures), we suggest that northern Ellesmere Island forms the northwestern continuation of the DeGeer Fault Zone and is thus, unlike the rest of Ellesmere Island, mostly controlled by movements between Greenland and the Barents Sea/Spitsbergen margin. Thus, northern Ellesmere Island/Pearya shows a fundamentally different response to Eurekan deformation than southern/central Ellesmere Island. As a boundary between the two exhumation regimes we tentatively propose the Mount Rawlingson Fault System (see also Piepjohn et al., 2016; their Figure 9), but due to lack of thermochronology data from central Ellesmere Island, this proposed boundary is poorly defined.

At ~48 Ma, exhumation of Pearya slowed down. At the same time, the Norwegian-Greenland Sea experienced a major plate tectonic reorganization (Gernigon et al., 2012). Spreading directions changed abruptly, associated with a strong decrease of spreading rates along the Mohns and Aegir Ridges (Gaina et al., 2009; Gernigon et al., 2012; Mosar et al., 2002). This new spreading regime prevailed until ~44 Ma, and likewise, exhumation rates of Pearya stagnated between 48 and 44 Ma.

At 44 Ma, the spreading direction of the Norwegian-Greenland Sea changed again (Gaina et al., 2009), and so did exhumation of Pearya, which again accelerated (Figure 7b). This time, however, the change of spreading direction and onset of more rapid exhumation of Pearya was not associated with an increase of spreading rates of the Norwegian-Greenland Sea, but to the contrary, with a further decrease. In contrast to the first stage of Eurekan deformation, where most of the movements of the Greenland plate were accommodated by transpression along the Svalbard/Barents Sea margin, Greenland was during that time pushed toward Ellesmere Island (Piepjohn et al., 2016). This convergence may have caused a slowdown of spreading rates of the Norwegian-Greenland Sea. Thus, it seems that the relationship between Eurekan deformation and North Atlantic spreading works in both directions: Seafloor spreading drove Eurekan deformation, but Eurekan deformation also influenced seafloor spreading. Also at this time, the northeastern margin of the Atlantic developed some mild compressional features (Ormen Lange Dome and Helland Hansen Arch; Doré et al., 2008), which may also be viewed in the general framework of changes in seafloor spreading and the effect of the Eurekan Greenland-Canada convergence.

Rapid exhumation of Pearya ceased at ~38 Ma, again roughly coeval with a change of spreading directions of the Norwegian-Greenland Sea (Gaina et al., 2009). Spreading rates slightly increased between 38 and 34 Ma, while exhumation of Pearya stagnated. Rapid exhumation of Pearya resumed at 34 Ma, again contemporaneous with a major plate tectonic reorganization of the North Atlantic realm: Spreading of the Labrador Sea/Baffin Bay ceased (Kristoffersen & Talwani, 1977), and so did the independent movement of Greenland, which became part of the North American plate (Tessensohn & Piepjohn, 2000; Figure 7c). As a consequence, Greenland and Europe started to move in different (absolute) directions (Gaina et al., 2009). This divergent movement also marks the end of the Eurekan Orogeny in a strict sense. The new plate tectonic situation may have triggered renewed (transtensional) movements along the DeGeer Fracture Zone between Greenland and Svalbard/Barents Sea and thus may have reactivated strike-slip movements in Pearya.

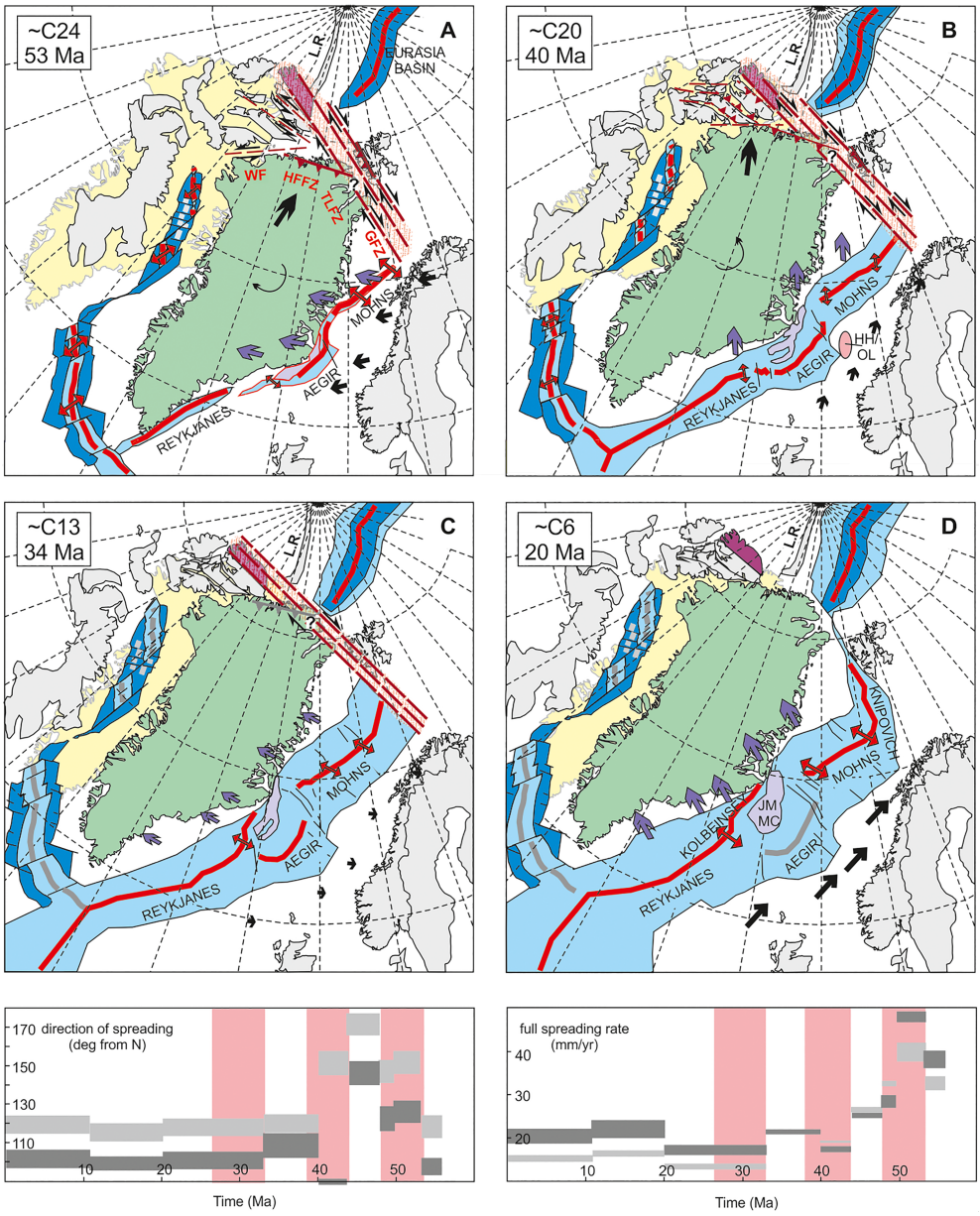

Figure 7. Paleogeographic reconstruction of the study area and its surroundings compiled after Lundin and Doré (2002), Mosar et al. (2002), Gaina et al. (2009), Tessensohn and Piepjohn (2000), Gernigon et al. (2012), Oakey and Chalmers (2012), Piepjohn et al. (2013, 2016), Anudu et al. (2016), Gion et al. (2017), and Newton and Huuse (2017). For reference, the present-day position of Greenland is shown in yellow. The Pearya Terrane/Northern Ellesmere Island is marked in purple. Violet and small black arrows: movements of Greenland and Europe, respectively, relative to a hot spot beneath Greenland, after Gaina et al. (2009). The movement of Greenland relative to North America, as well as the resultant rotation of Greenland due to seafloor spreading east and west of Greenland, is illustrated with black arrows on Greenland plate (modified after Tessensohn & Piepjohn, 2000). Red arrows display the direction of extension along the spreading ridges. Dark blue: Paleocene oceanic areas; light blue: Eocene and post-Eocene oceanic areas; red thick lines: active spreading ridges and fault zones; gray thick lines: inactive spreading ridges and fault zones. HFFZ: Harder Fjord Fault Zone; the Trolle Land Fault Zone (TFFZ) and Greenland Fracture Zone (GFZ) are interpreted as part of the DeGeer Fault Zone in a strict sense; WF: Wegener Fault; Dashed polygon: strike-slip/transform fault zone discussed in the text. JMMC: Jan Mayen Microcontinent; HH: Helland Hansen Arch; OM: Ormen Lange Dome; L.R.: Lomonosov Ridge. Iceland and parts of the Canadian Arctic Archipelago have been deliberately omitted for the sake of simplicity and since it not playing a critical role on the under investigation relative movements of Greenland from 12Eocene times onward. (a) Situation during the first stage of rapid Eurekan exhumation on Pearya. (b) Situation during the second stage of rapid Eurekan exhumation. (c) Situation during the post-Eurekan stage of rapid exhumation. (d) Situation when rapid exhumation has ceased and Pearya is decoupled from movements along the DeGeer Fault Zone. Lower part (graphs): Changes of spreading directions and spreading rates through time for the northern NE Atlantic (light gray) and the southern NE Atlantic (dark gray) from Gaina et al. (2009), compared to period of rapid exhumation on Pearya (rose-colored).

Rapid exhumation of Pearya finally ceased at ~26 Ma. This change in exhumation rates may be coincident with a ridge jump in the Norwegian-Greenland Sea, with the Aegir Ridge finally becoming inactive, and spreading instead focusing along the Kolbeinsey Ridges, which led to separation of the Jan Mayen Microcontinent from Greenland (Lundin & Doré, 2002; Vogt et al., 1980; Figure 7d). Timing of this event, however, is poorly constrained. Probably more important for the exhumation history of Pearya, the Mohns Ridge experienced a change of spreading direction from NNW-SSE toward NW-SE, which may have been associated with the onset of seafloor spreading along the Knipovich Ridge (Vogt et al., 1982). Spreading of the Knipovich Ridge connected the spreading systems of the Norwegian-Greenland Sea with the Gakkel Ridge of the Arctic Ocean, thus finally separating Svalbard from Greenland (Figure 7d). However, timing of spreading activity along the Knipovich Ridge is still debated. In any case, if our suggestion that Pearya movements are coupled to movements along the DeGeer Fracture Zone is correct, then the final cessation of rapid exhumation of Pearya seems to indicate its final decoupling from the DeGeer Fracture Zone.

5.3. Relationship to Environmental Changes of the Arctic

The first, >55–48-Ma period of Eurekan exhumation took place under warm and humid conditions (Figure 6), as evidenced by our palynological data, and in agreement with data from other parts of the Arctic (e.g., Eberle & Greenwood, 2012; Sluijs et al., 2006). The Eurekan Belt of Pearya underwent active erosion of at least 2–3 km at that time, suggesting that substantial topography already existed. On the other hand, our data also show that at least at the start of this first exhumation period, parts of the present-day continental margin were still characterized by low-lying topography and coastal basins at sea level until at least 54 Ma.

The second stage of Eurekan exhumation between ~44 and 38 Ma presumably also affected the sedimentary basins, which became deformed and eroded (Piepjohn et al., 2013), suggesting that general uplift and topographic growth became more pronounced during this stage. Contemporaneously, IRD was deposited off East Greenland, indicating continental glaciation of the sediment source area, with first IRD observed from 44 Ma onward (Tripati et al., 2008), and peak occurrences between 40 and 38 Ma. Also at the same time, however, dense *Metasequoia* forests prevailed on Axel Heiberg Island adjacent to Ellesmere Island (and both islands were already situated at nearly the same latitude as they are today; Jahren & Sternberg, 2008), and mean annual air temperatures of Greenland were ~13 to 15 °C (Schouten et al., 2008). The apparent contradiction between lush Arctic vegetation and relatively high temperatures on the one hand, and the existence of continental ice on the other hand, may be resolved by assuming that glaciation was focused on areas with high-standing topography, as it very likely existed along the Eurekan Belt stretched along the northern continental margin of Canada and Greenland and along the western margin of Spitsbergen. Also, ice sheet models require a topographic increase of ~1–1.5 km compared to the present day for simulating continental glaciation under the warmer Eocene climate (Langebroek et al., 2017).

Previous studies assume that chiefly the East Greenland coast between ~69 and 75°N (referring to present-day position) was affected by Eocene glaciation (Eldrett et al., 2007). This assumption is based on the lithologies of IRD in the offshore deposits, comprising mostly basalts, quartzites, and gneisses. These have been correlated with Paleogene flood basalts and Proterozoic metasedimentary rocks exposed along the East Greenland coast (Eldrett et al., 2007). However, similar rock types also occur farther north in the Eurekan belt of Greenland and Canada. Moreover, thermochronology data from the East Greenland continental margin between 68 and 76°N indicate increased glacial erosion from 30 ± 5 Ma onward (Bernard et al., 2016), postdating offshore occurrences of IRD. Based on the temporal coincidence between IRD deposition and rapid exhumation (and thus presumably topography building; Figure 6) along the Eurekan belt, we suggest that continental glaciation initiated in the Eurekan areas of Greenland and Pearya, about 1,300 km farther north than previously assumed. Glacially eroded debris from the southeastern side of the Eurekan Belt may have been transported toward the sea and then by icebergs along the—already marine, although not deep oceanic (Torsvik & Cocks, 2016)—areas of the present-day Greenland coastline towards the south, where it finally became deposited off the East Greenland coast. We furthermore speculate that the initial icecap nucleating in the Eurekan belt may have subsequently extended farther to the south, causing glaciation of the East Greenland margin at the Eocene-Oligocene boundary associated with renewed deposition of IRD at ~32–30 Ma (Eldrett et al., 2007; Figure 6). Based on magnetic properties, Eldrett et al. (2007) suggest different source terranes for the Eocene versus Oligocene IRD, which would be in agreement with glacial expansion from the Eurekan belt toward the south, along the East Greenland coast. However, more

detailed IRD provenance studies and investigations on the onshore glacial evolution are required to (dis) prove these interpretations.

6. Conclusions

Based on our effort to shed light on the evolution of the Eurekan belt of Pearya by studying its bedrock exposures and syntectonic sediments, we derive the following conclusions:

1. During its pre-Cenozoic history, Pearya has experienced exhumation periods associated with the Carboniferous Ellesmerian orogeny followed by the Sverdrup basin formation and with the Early Cretaceous opening of the Amerasia Basin. During the Paleocene, Pearya was again characterized by rapid denudation most likely associated with crustal stretching, which led to basin formation and deposition of the Eureka Sound Group in a marine-influenced, coastal swamp environment.
2. The exhumational response to Eocene Eurekan deformation was strongly focused in the north: While Eurekan-deformed areas of southeast Ellesmere Island experienced less than 2–3-km exhumation, the basement rocks of Pearya were characterized by 8–11 km of exhumation.
3. Eurekan (and post-Eurekan) exhumation was episodic, with periods of enhanced exhumation between ~55 and 48 Ma, and ~44–38 Ma, and ~34–26 Ma, and periods of quiescence in between. We correlate these periods of enhanced exhumation with periods of strike-slip faulting in Pearya and with changes of spreading rates and movements directions of the North Atlantic Ocean.
4. We suggest that Pearya forms the northwestern continuation of the DeGeer Fracture Zone, and thus, unlike the rest of Ellesmere Island, Pearya's exhumation history is connected to movements between Northeast Greenland and Svalbard.
5. Rapid exhumation of Pearya ceased at ~26 Ma. This change in exhumation rates is interpreted as reflecting the final decoupling of Pearya from strike-slip movements along the De Geer Fracture Zone, associated with the incipient opening stages of the future Fram Strait.
6. The early phase of Eurekan exhumation of Pearya occurred under warm and humid climate conditions. Parts of the Canadian margin were still topographically subdued, forming basins that received detritus from the exhuming Eurekan belt.
7. The second period of Eurekan exhumation also affected the former sedimentary basins. Rapid exhumation during the Eurekan (second stage) and post-Eurekan temporally coincided with deposition of IRD offshore Greenland. We thus suggest that the high-latitude Eurekan belt provided the topography required to allow for continental glaciation under the warmer climate of the Eocene. We further speculate that the Eurekan belt formed the nucleus for glacier formation, which extended further to the south at around the Eocene-Oligocene boundary.

Acknowledgments
The fieldwork for the study was organized and financed by the BGR as part of the CASE program. We furthermore received funding from the German Science Foundation (DFG), project SP 673/23-1. All the data supporting our results and conclusions can be found in the information system PANGAEA (doi.pangaea.de/10.1594/PANGAEA.905014) and in the Supporting Information (SI) file. We would like to thank the CASE 11 expedition team and the Polar Continental Shelf Program (Resolute Bay, Nunavut, Canada) for logistic support during field work. We also thank the field guides, helicopter pilots, and cook/camp manager, who took care of logistics and safety measures during the field campaign. P. Bijl and J. Frieling from Utrecht University are thanked for discussions on palynostratigraphy. We also acknowledge V. Kolb, Chr. Schott, A. Toltz, A. Hübner, and K. Meier from University of Bremen, for technical support. Detailed and constructive reviews by Grace Shephard (University of Oslo) and Randell Stephenson (University of Aberdeen) and editorial handling by Taylor Schildgen (GFZ Potsdam) greatly improved an earlier version of this paper.

References

Alvey, A., Gaina, C., Kusznir, N. J., & Torsvik, T. H. (2008). Integrated crustal thickness mapping and plate reconstructions for the high Arctic. *Earth and Planetary Science Letters*, *271*, 310–321. https://doi.org/10.1016/j.epsl.2008.07.036

Anudu, G. K., Stephenson, R. A., Macdonald, D. I. M., & Oakey, G. N. (2016). Geological features of the north-eastern Canadian Arctic margin revealed from analysis of potential field data. *Tectonophysics*, *691*, 48–64.

Arne, D., Grist, A., ZEntilli, M., Collins, M., Embry, A., & Gentzis, T. (2002). Cooling of the Sverdrup Basin during Tertiary basin inversion: Implications for hydrocarbon exploration. *Basin Research*, *14*(2), 183–205. https://doi.org/10.1046/j.1365-2117.2002.00163.x

Arne, D., Zentilli, M., Grist, A., & Collins, M. (1998). Constraints on the timing of thrusting during the Eurekan orogeny, Canadian Arctic Archipelago: An integrated approach to thermal history analysis. *Canadian Journal of Earth Sciences*, *35*(1), 30–38. https://doi.org/10.1139/e97-088

Backman, J., Jakobsson, M., Frank, M., Sangiorgi, F., Brinhuis, H., Stickley, C., et al. (2008). Age model and core-seismic integration for the Cenozoic Arctic Coring Expedition sediments from the Lomonosov Ridge. *Paleoceanography*, *23*, PA1S03. https://doi.org/10.1029/2007PA001476

Bernard, T., Steer, P., Gallagher, K., Szilc, A., Whitham, A., & Johnson, C. (2016). Evidence for Eocene–Oligocene glaciation in the landscape of the East Greenland margin. *Geology*, *44*, 895–898.

Blythe, A. E., & Kleinspehn, K. (1998). Tectonically versus climatically driven Cenozoic exhumation of the Eurasian Plate Margin, Svalbard; Fission Track Analyses. *Tectonics*, *17*, 621–639.

Brandon, M., 2007. BinomFit for Windows, version 1.2.63. Program to decompose mixed grain-age distributions for fission-track dating. Created by Mark Brandon and Igor Boreyko. Yale University 2002, 2007. http://www.geology.yale.edu/~brandon

Brozena, J., Childers, V., Lawver, L., Gahagan, L., Forsberg, R., Faleide, J., & Eldholm, O. (2003). New aerogeophysical study of the Eurasia Basin and Lomonosov Ridge: Implications for basin development. *Geology*, *31*, 825–828.

Bujak, J., & Mudge, D. (1994). A high-resolution North Sea Eocene dinocyst zonation. *Journal of the Geological Society, London*, *151*, 449–462.

De Geer, G. (1909). Some leading features of dislocation in Spitzbergen. *GFF*, *31*, 199–208.

Doré, A., Lundin, E., Kusznir, N., & Pascal, C. (2008). Potential mechanisms for the genesis of Cenozoic dome structures on the NE Atlantic margin: Pros, cons and some new ideas. *Geological Society, London, Special Publications*, *306*, 1–26.

Dörr, N., Lisker, F., Jochmann, M., Rainer, T., Schlegel, A., Schubert, K., & Spiegel, C. (2019). Subsidence, rapid inversion and slow erosion of the Central Tertiary Basin of Svalbard: Evidence from the thermal evolution and basin modeling. In K. Piepjohn, J. Strauss, L. Reinhardt, & W. McClelland (Eds.), *Circum-Arctic structural events: Tectonic evolution of the Arctic margins and trans-Arctic links with adjacent orogens: Geological Society of America Special Paper*, (Vol. 541, pp. 169–188).

Dunkl, I. (2002). Trackkey: A Windows program for calculation and graphical presentation of fission track data. *Computer & Geosciences*, *28*(1), 3–12.

Eberle, J. E., & Greenwood, D. R. (2012). Life at the top of the greenhouse Eocene world—A review of the Eocene flora and vertebrate fauna from Canada's High Arctic. *Geological Society of America Bulletin*, *124*, 3–23.

Eldrett, J., Harding, I., Wilson, P., Butler, E., & Roberts, A. (2007). Continental ice in Greenland during the Eocene and Oligocene. *Nature*, *446*, 176–179.

Embry, A., & Osadetz, K. (1988). Stratigraphy and tectonic significance of Cretaceous volcanism in the Queen Elizabeth Islands, Canadian Arctic Archipelago. *Canadian Journal of Earth Sciences*, *25*(8), 1209–1219. https://doi.org/10.1139/e88-118

Estrada, S., Henjes-Kunst, F., & Höhndorf, A. (1999). Cretaceous volcanites from the Canaclian Arctic islands: Magmatism related to the opening of the Arctic Ocean. *Ber. Deut. Mineral. Gesell., Beih. Eur. J. Mineral*, *11*(1), 66.

Estrada, S., Mende, K., Gerdes, A., Gärtner, A., Hofmann, M., Spiegel, C., et al. (2018). Proterozoic to Cretaceous evolution of the western and central Pearya Terrane (Canadian High Arctic). *Journal of Geodynamics*, *120*, 45–76.

Estrada, S., Piepjohn, K., Frey, M. J., Reinhardt, L., Andruleit, H., & von Gosen, W. (2009). Pliocene coal-seam fires on southern Ellesmere Island, Canadian Arctic. *Neues Jahrbuch für Geologie und Paläontologie, Abhandlungen*, *251*(1), 33–52. http://doi.org/10.1127/0077-7749/2009/0251-0033

Estrada, S., Piepjohn, K., Henjes-Kunst, F., & Gosen, W. von (2006). Geology, magmatism and structural evolution of the Yelverton Bay area, northern Ellesmere Island. *Arctic Canada. – Polarforschung*, *73*(2/3), 59–75.

Farley, K. (2000). Helium diffusion from apatite. General behavior as illustrated by Durango fluorapatite. AGU, Journal of Geophysical Research. *Solid Earth*, *105*(B2), 2903–2014.

Farley, K. (2002). (U-Th)/He dating: Techniques, calibrations, and applications, in: Noble gases in geochemistry and cosmochemistry. *Reviews in Mineralogy & Geochemistry*, *47*(1), 819–844.

Farley, K., Wolf, R., & Silver, L. (1996). The effects of long alpha-stopping distances on (U-Th)/He ages. *Geochimica et Cosmochimica Acta*, *60*(21), 4223–4229.

Frieling, J., Iakovleva, A. I., Reichart, G. J., Aleksandrova, G. N., Gnibidenko, Z. N., Schouten, S., & Sluijs, A. (2014). Paleocene–Eocene warming and biotic response in the epicontinental West Siberian Sea. *Geology*, *42*, 767–770.

Gaina, C., Gernigon, L., & Ball, P. (2009). Palaeocene-Recent plate boundaries in the NE Atlantic and the formation of the Jan Mayen microcontinent. *Journal of the Geological Society, London*, *166*, 601–616.

Galbraith, R. F., & Laslett, G. M. (1993). Statistical models for mixed fission track ages. *Nuclear tracks and radiation measurements*, *21*, 459–470.

Gernigon, L., Gaina, C., Olesen, O., Ball, P., Péron-Pinvidic, G., & Yamasaki, T. (2012). The Norway Basin revisited: From continental breakup to spreading ridge extinction. *Marine and Petroleum Geology*, *35*, 1–19.

Gion, A., Williams, S., & Müller, D. (2017). A reconstruction of the Eurekan Orogeny incorporating deformation constraints. *Tectonics*, *36*, 304–320. https://doi.org/10.1002/2015TC004094

Gleadow, A. J. W. (1981). Fission track dating methods: What are the real alternatives? *Nuclear tracks and radiation measurements*, *5*, 3–14.

Gradstein, F. M., Ogg, J. G., Schmitz, M., & Ogg, G. (2012). *The geologic time scale 2012*, (p. s). Amsterdam: Elsevier.

Grist, A., & Zentilli, M. (2005). The thermal history of the Nares Strait, Kane Basin, and Smith Sound region in Canada and Greenland: Constraints from apatite fission-track and (U-Th-Sm)/He dating. *Canadian Journal of Earth Sciences*, *42*, 1547–1569.

Håkansson, E., & Pedersen, S. A. S. (2001). The Wandel Hav strike–slip mobile belt—A Mesozoic plate boundary in North Greenland. *Bulletin of the Geological Society of Denmark*, *48*, 149–158.

Hansen, K., Dawes, P., Frisch, T., & Jensen, P. (2011). A fission track transect across Nares Strait (Canada-Greenland): Further evidence that the Wegener Fault is a myth. *Canadian Journal of Earth Sciences*, *48*, 819–840.

Harland, W. B. (1969). Contribution of Spitsbergen to understanding of tectonic evolution of North Atlantic region. In M. Kay (Ed.), *North Atlantic—Geology and continental drift, AAPG Memoirs*, (Vol. 12, pp. 817–851).

Harrison, J. C. (2006). In search of the Wegener Fault: Re-evaluation of strike-slip displacements along and bordering Nares Strait. *Polarforschung*, *74*(1–3), 129–160.

Hurford, A. J., & Green, P. F. (1983). The zeta age calibration of fission track dating. *Chemical Geology*, *41*(4), 285–317.

Jahren, A., & Sternberg, L. (2008). Annual patterns within tree rings of the Arctic middle Eocene (ca. 45 Ma): Isotopic signatures of precipitation, relative humidity, and deciduousness. *Geology*, *36*, 99–102.

Jakobsson, M., Macnab, R., Mayer, L., Anderson, R., Edwards, M., Hatzky, J., et al. (2008). An improved bathymetric portrayal of the Arctic Ocean: Implications for ocean modeling and geological, geophysical and oceanographic analyses. *Geophysical Research Letters*, *35*, L07602. https://doi.org/10.1029/2008gl033520

Jones, M. T., Augland, L. E., Shephard, G. R., Burgess, S. D., Gauti, T. E., Jochmann, M. M., et al. (2017). Constraining shifts in North Atlantic plate motions during the Palaeocene by U-Pb dating of Svalbard tephra layers. *Nature, Scientific Reports*, *7*, 6822. https://doi.org/10.1038/s41598-017-06170-7

Ketcham, R. (2005). Forward and inverse modeling of low-temperature thermochronometry data. *Reviews Mineralogy Geochemistry*, *58*, 275–314.

Ketcham, R., Carter, A., Donelick, R., Barbarand, J., & Hurford, A. (2007a). Improved modeling of fission-track annealing in apatite. *American Mineralogist*, *92*, 799–810.

Ketcham, R., Carter, A., Donelick, R., Barbarand, J., & Hurford, A. (2007b). Improved measurement of fission track annealing in apatite using c-axis projection. *American Mineralogist*, *92*, 789–798.

Ketcham, R., Gautheron, C., & Tassan-Got, L. (2011). Accounting of long alpha-particle stopping distances in (U-Th-Sm)/He geochronology: Refinement of the baseline case. *Geochimica et Cosmochimica Acta*, *75*, 7779–7791.

Ketcham, R. A., Carter, A., & Hurford, A. J. (2015). Inter-laboratory comparison of fission track confined length and etch figure measurements in apatite. *American Mineralogist*, *100*, 1452–1468.

Kristoffersen, Y., & Talwani, M. (1977). Extinct triple junction south of Greenland and the Tertiary motion of Greenland relative to North America. *Geological Society of America Bulletin*, *88*, 1037–1049.

Langebroek, P., Nisancioglu, K., Lunt, D., Pedersen, V., Meckler, N., & Gasson, E. (2017). 2017. On the possibility of ice on Greenland during the Eocene-Oligocene transition. *Geophysical Research Abstracts*, *19*, EGU2017–EGU3163.
Lundin, E., & Doré, A. (2002). Mid-Cenozoic post-breakup deformation in the "passive" margins bordering the Norwegian-Greenland Sea. *Marine and Petroleum Geology*, *19*, 79–93.
Lyberis, N., & Manby, G. (2001). The Eurekan deformation of North and Eastern North Greenland. *Polarforschung*, *69*, 95–106.
McDowell, F., McIntosh, W., & Farley, K. (2005). A precise ^{40}Ar-^{39}Ar reference age for the Durango apatite (U-Th)/He and fission track dating standard. *Chemical Geology*, *214*, 249–263.
Miall, A. D. (1986). The Eureka Sound Group (Upper Cretaceous-Oligocene). *Canadian Arctic Islands: Bulletin of Canadian Petroleum Geology*, *34*, 240–270.
Mosar, J., Eide, E., Osmundsen, P., Sommaruga, A., & Torsvik, T. (2002). Greenland-Norway separation: A geodynamic model for the North Atlantic. *Norwegian Journal of Geology*, *82*, 281–298.
Newton, A., & Huuse, M. (2017). Late Cenozoic environmental changes along the Norwegian margin. *Marine Geology*, *393*, 216–244.
Oakey, G., & Chalmers, J. (2012). A new model for the Paleogene motion of Greenland relative to North America: Plate reconstructions of the Davis Strait and Nares Strait regions between Canada and Greenland. *Journal of Geophysical Research*, *117*, B10401. https://doi.org/10.1029/2011jb008942
O'Regan, M., Moran, K., Backman, J., Jakobsson, M., Sangiorgi, F., Brinkhuis, H., et al. (2008). Mid-Cenozoic tectonic and paleoenvironmental setting of the Central Arctic Ocean. *Paleoceanography*, *23*, PA1S20. https://doi.org/10.1029/2007PA001559
Piepjohn, K., von Gosen, W., Läufer, A., McClelland, W., & Estrada, S. (2013). Ellesmerian and Eurekan fault tectonics at the northern margin of Ellesmere Island (Canadian High Arctic). *Zeitschrift der Deutschen Gesellschaft für Geowissenschaften*, *164*(1), 81–106.
Piepjohn, K., von Gosen, W., & Tessensohn, F. (2016). The Eurekan deformation in the Arctic: An outline. *Journal of the Geological Society*, *173*, 1007–1024.
Piepjohn, K., von Gosen, W., Tessensohn, F., Reinhardt, L., McClelland, W., Dallmann, W., et al. (2015). Tectonic map of the Ellesmerian and Eurekan deformation belts on Svalbard, North Greenland, and Queen Elizabeth Islands (Canadian Arctic). *Arktos*, *1*(1), 12, 7 p. https://doi.org/10.1007/s41063-015-0015-7
Poirier, A., & Hillaire-Marcel, C. (2011). Improved Os-isotope stratigraphy of the Arctic Ocean. *Geophysical Research Letters*, *38*, 2011GL047953. https://doi.org/10.1029/2011gl047953
Pross, J. (2001). Paleo-oxygenation in Tertiary epeiric seas: Evidence from dinoflagellate cysts. *Palaeogeography, Palaeoclimatology, Palaeoecology*, *166*, 369–381.
Ricketts, B. (1994). Basin analysis, Eureka Sound Group, Axel Heiberg and Ellesmere Islands. *Canadian Arctic Archipelago. Geological Survey of Canada Memoir*, *439*, 119.
Ricketts, B., Osadetz, K. G., & Embry, A. F. (1985). Volcanic style in the Strand Fiord Formation (Upper Cretaceous), Axel Heiberg Island, Canadian Arctic Archipelago. *Polar Res.*, *3*(1), 107–122.
Ricketts, B. D., & Stephenson, R. A. (1994). The demise of Sverdrup Basin: Late Cretaceous-Paleogene sequence stratigraphy and forward modelling. *Journal of Sedimentary Research B: Stratigraphy and Global Studies*, *B64*, 516–530.
Schouten, S., Eldrett, J., Greenwood, D., Harding, I., Baas, M., & Sinninghe Damsté, J. (2008). Onset of long-term cooling of Greenland near the Eocene-Oligocene boundary as revealed by branched tetraether lipids. *Geology*, *36*(2), 147–150.
Shephard, G., Müller, D., & Seton, M. (2013). The tectonic evolution of the Arctic since Pangea breakup: Integrating constraints from surface geology and geophysics with mantle structure. *Earth Science Reviews*, *124*, 148–183.
Sluijs, A., Schouten, S., Pagani, M., Woltering, M., Brinkhuis, H., Damsté, J. S., et al. (2006). Subtropical Arctic Ocean temperatures during the Palaeocene/Eocene thermal maximum. *Nature*, *441*(7093), 610–613. https://doi.org/10.1038/nature04668
Srivastava, S. P. (1978). Evolution of the Labrador Sea and its bearing on the early evolution of the North Atlantic. *Geophysical Journal of the Royal Astronomic Society*, *52*, 313–357.
Stein, R., Weller, P., Backman, J., Brinkhuis, H., Moran, K., & Pälike, H. (2014). Cenozoic Arctic Ocean climate history: Some highlights from the Integrated Ocean Drilling Program Arctic Coring Expedition. *Developments in Marine Geology*, *7*, 259–293.
Stickley, C., St John, K., Koc, N., Jordan, R., Passchier, S., Pearce, R., & Kearns, L. (2009). Evidence for middle Eocene Arctic sea ice from diatoms and ice-rafted debris. *Nature*, *460*, 376–380.
Tailleur, I. L. (1973). Probable rift origin of the Canada Basin. In M. G. Pitcher (Ed.), *Arctic Geology: American Association of Petroleum Geologists Memoir* (Vol. 19, pp. 526–535). AAPG: Tulsa.
Tegner, C., Storey, M., Holm, P., Thorarinsson, S., Zhao, X., Lo, C., & Knudsen, M. (2011). Magmatism and Eurekan deformation in the High Arctic Large Igneous Province: ^{40}Ar-^{39}Ar age of Kap Washington Group volcanics, North Greenland. *Earth and Planetary Science Letters*, *303*, 203–214.
Tessensohn, F., & Piepjohn, K. (2000). Eocene compressive deformation in Arctic Canada, North Greenland and Svalbard and its plate tectonic causes. *Polarforschung*, *68*, 121–124.
Thorsteinsson, R., & Tozer, E. T. (1970). Geology of the Arctic Archipelago. In R. J. W. Douglass (Ed.), *Geology and economic minerals of Canada. Geological Survey of Canada, Economic Geology Report*, (Vol. 1, pp. 547–590).
Torsvik, T., & Cocks, L. (2016). Paleogene. In *Earth history and palaeogeography*, (pp. 240–255). Cambridge: Cambridge University Press. https://doi.org/10.1017/9781316225523.015
Trettin, H. (1991). Geology of the Innuitian Orogen and Arctic platform of Canada and Greenland. *Geol. Canada*, *3*.
Trettin, H. P. (1998). Pre-Carboniferous geology of the northern part of the Arctic islands. Chapter 4: Geology of Pearya. *Geological Survey of Canada, Bulletin*, *425*, 108–192.
Trettin, H.P., and Frisch, T.O., 1996. Geology, Yelverton Inlet, Map 1881A, Scale 1:250,000.Geological Survey of Canada.
Trettin, H. P., & Mayr, U. (1996). Geological map of Lady Franklin Bay, District of Franklin, Northwest Territories, 1:250,000. *Geological Survey of Canada, Map*, *1887A*.
Tripati, A., Eagle, R., Morton, A., Dowdeswell, J., Atkinson, K., Bahé, Y., et al. (2008). Evidence for glaciation in the Northern Hemisphere back to 44 Ma from ice-rafted debris in the Greenland Sea. *Earth and Planetary Science Letters*, *265*, 112–122.
Vogt, P., Johnson, G., & Krisjannson, L. (1980). Morphology and magnetic anomalies north of Iceland. *Journal of Geophysics*, *47*, 67–80.
Vogt, P., Kovacs, L., Bernero, C., & Srivastava, S. (1982). Asymmetric geophysical signatures in the Greenland-Norwegian and southern Labrador Seas and the Eurasia Basin. *Tectonophysics*, *89*, 95–160.
von Gosen, W., & Piepjohn, K. (2003). Eurekan transpressive deformation in the Wandel Hav Mobile Belt (northeast Greenland). *Tectonics*, *22*(4), 2001TC901040. https://doi.org/10.1029/2001TC901040
von Gosen, W., Piepjohn, K., & Reinhardt, L. (2012). Polyphase Eurekan deformation along the Vendom Fiord Fault Zone on south Ellesmere Island (Canadian Arctic) and its possible relation to the Wegener Fault. *German, Journal of Geosciences*, *163*, 261–282.

Wagner, G., Gleadow, A., & Fitzgerald, P. (1989). The significance of the partial annealing zone in apatite fission track analysis: projected track lengths measurement and uplift chronology of the Tranantarctic Mountains. *Chemical Geology*, *79*(4), 295–305.

Williams, G. L., Brinkhuis, H., Pearce, M. A., Fensome, R. A., & Weegink, J. W. (2004). Southern Ocean and global dinoflagellate cyst events compared: index events for the Late Cretaceous-Neogene. In N. F. Exon, J. P. Kennett, & M. J. Malone (Eds.), *Proceedings of the Integrated Ocean Drilling Program, Scientific Results* (Vol. 189, pp. 1–98). College Station: Ocean Drilling Program-TX. https://doi:10.2973/odp.proc.sr.189.107.2004

Wilson, D., 1976. Eureka Sound and Beaufort formations, Yelverton Bay, Ellesmere Island, District of Franklin. Geological Survey of Canada, Paper 76-1A (Report of Activities) 453–456.

Wolf, R. A., Farley, K. A., & Kass, D. M. (1998). Modeling of the temperature sensitivity of the apatite (U-Th)/He thermochronometer. *Chemical Geology*, *148*, 105–114.

Zachos, J., Pagani, M., Sloan, L., Thomas, E., & Billups, K. (2001). Trends, rhythms, and aberrations in global climate 65 Ma to present. *Science*, *292*, 686–693.